CHAPTER - 4

EXTRACTION OF METALS FROM SPENT NICKEL-METAL HYDRIDE BATTERIES

Extraction of metals from spent nickel-metal hydride batteries

Besides the base metals such as Ni, Co, Fe, Mn and Zn, the nickel-metal hydride batteries (Ni-MH) are rich in valuable rare earth metals (REMs) viz. La, Sm, Nd, Pr and Ce as well as mentioned in Chapter-II. In order to achieve the objectives of resource recycling and assured supply of the contained metals of this waste, the hydrometallurgical processing of spent Ni-MH batteries is investigated in this chapter with a focus on the recovery of both the base and rare earth metals.

4.1 Leaching of base metals from spent NiMH batteries

Because of the ease of handling, lesser gaseous pollution and requirement of simple material of construction, sulfuric acid may be considered as the leaching medium, although some experiments with HCl have also been performed. Accordingly, the leaching of base metals from the electrode powder of NiMH batteries is investigated in detail with emphasis on the kinetics and mechanism of the metal dissolution, which is followed by the characterization studies using XRD and SEM-EDAX techniques.

4.1.1 *Leaching of metals using different acids:* In order to examine the effect of different lixiviants on the leaching of metals from the NiMH battery material, initial experiments were conducted using mineral acids such as HCl and H_2SO_4 while varying the concentration from 0.5 to 3 M at 348 K, 500 rpm and 100 g/L pulp density for 120 min. Fig. 4.1 shows the increase in leaching efficiency of the metals. As can be seen the recovery of all metals increased with increase in acid concentration irrespective of the acid used (Rubisov et al., 2000). The leaching of 90.3% Ni and Co, 72.5% Fe, 91.3% Mn and 96% Zn was recorded using 3 M HCl in 120 min (Fig. 4.1a).

As regards the leaching with sulfuric acid, the metal dissolution increased with the increase in the acid concentration till 2 M H_2SO_4 and thereafter the leaching efficiency of all metals became almost constant (Fig. 4.1b). With 2 M H_2SO_4 leaching of 91.6% Ni, 97.8% Co, 93.5% Mn, 99.2% Zn and only 65.5% Fe was recorded at 100 g/L pulp density and 348 K in 120 min. Besides other advantages mentioned above, higher leaching efficiency of all metals and relatively low iron contamination of the leach solution are in favour of using sulfuric acid as the lixiviant compared to HCl.

The leaching reactions of the base metals present in the spent battery material with H_2SO_4 may be presented as (4.1-4.3):

$$M(OH)_2 + H_2SO_4 \rightarrow MSO_4 + 2H_2O \quad (4.1)$$

where M = Ni, Co, Mn and Zn. The dissolution of manganese containing phases can proceed as:

$$Mn_2O_3 + H_2SO_4 \rightarrow MnO_2 + MnSO_4 + H_2O \quad (4.2)$$

$$Mn_3O_4 + 2H_2SO_4 \rightarrow MnO_2 + 2MnSO_4 + 2H_2O \quad (4.3)$$

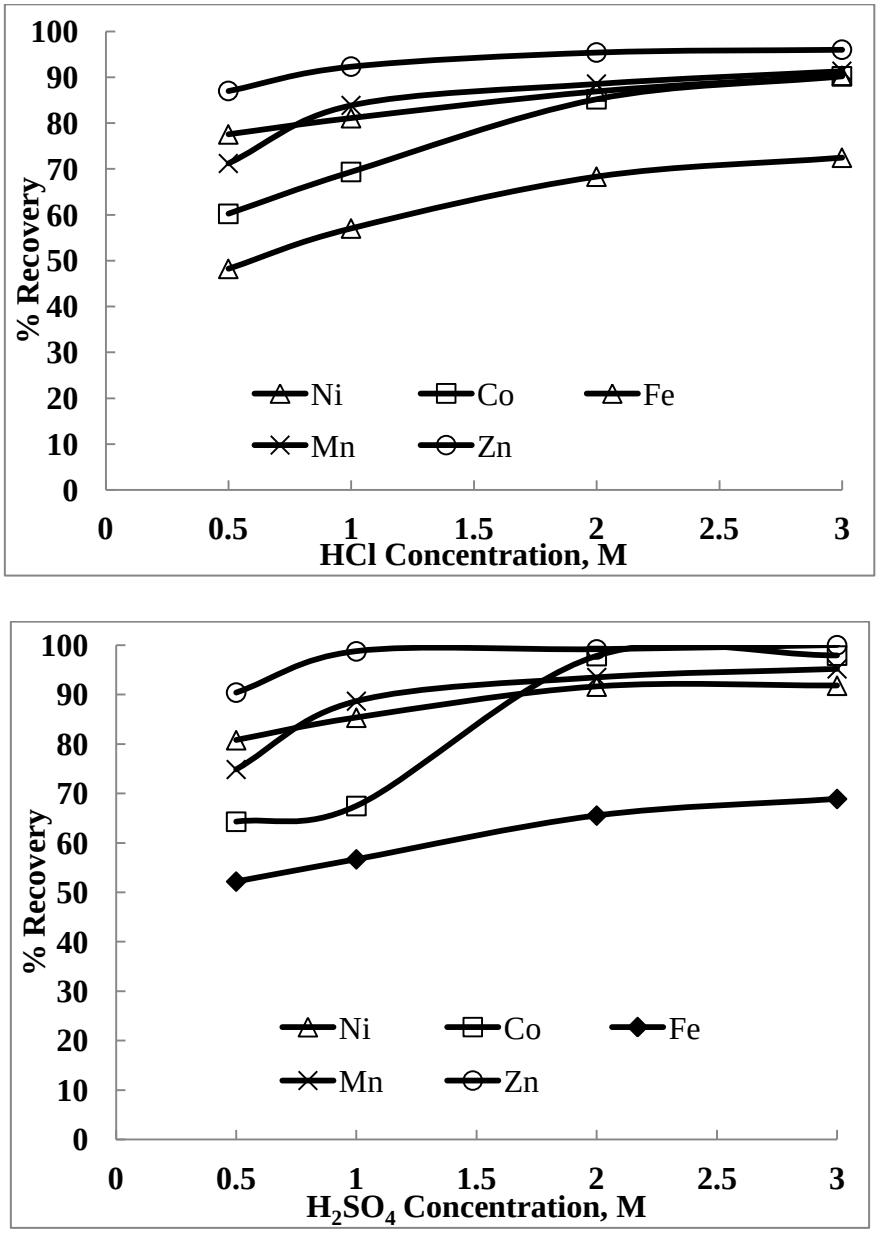

Fig. 4.1: Effect of acid concentration (a) HCl and (b) H_2SO_4 on the leaching efficiency of spent Ni-MH battery powder [S/L = 100 g/L, t: 120 min., T: 348 K]

4.1.2 *Effect of leaching time:* The effect of time on the leaching of metals was examined under the conditions mentioned in Fig. 4.2. Results show that the leaching efficiency of nickel reached ~57% in 60 min and the maximum recovery (~92%) was obtained in 120 min. Similarly leaching efficiency of Co, Fe, Mn and Zn was found to be 74.8, 37.4, 79.5 and 83.3%, respectively in 60 min; respective metal recovery being maximum of 97.8, 65.5, 93.5 and 99.2% in 120 min. The Ni dissolution was not that high as the electrode material utilized in this work consists of a highly porous screen type metallic network into which the nickel compounds are impregnated (Bertuol et al., 2006; Vegliò et al., 2003; Pietrelli et al., 2005). The residue obtained after filtration consists of nickel in the metallic phase or a complex oxide of Ni and Co as analysed by XRD analysis (Table 4.2) which are more resistant to the leaching under the conditions mentioned above. This may require the use of higher temperature, acid strength and oxidising conditions to achieve adequate solubilization in reasonable time (Nogeira and Margarido, 2004).

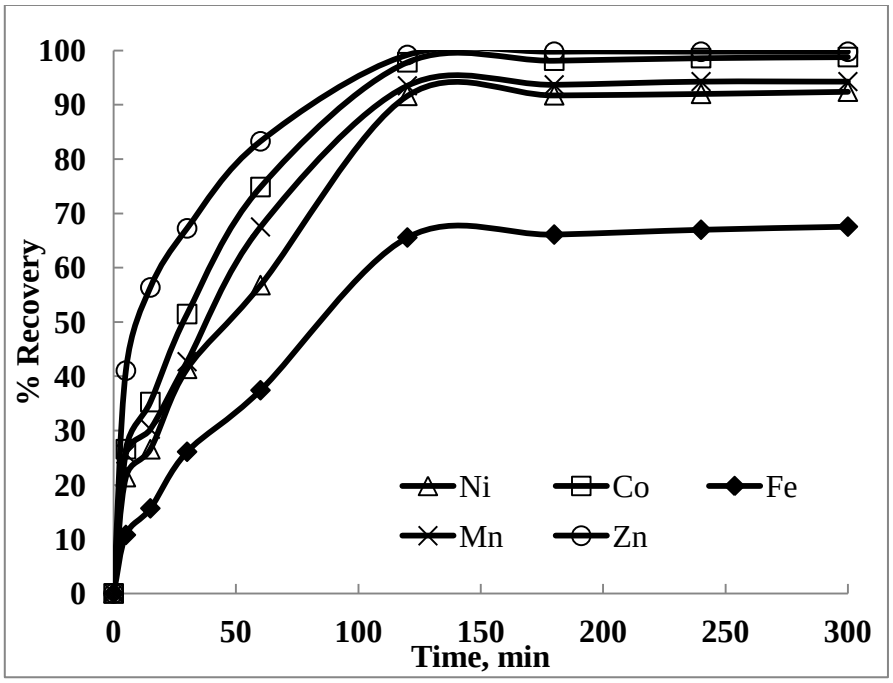

Fig. 4.2: Effect of time on the leaching efficiency of electrode powder [Acid: 2 M H_2SO_4, T: 348 K, S/L =100 g/L]

4.1.3 *Effect of stirring speed*: Effect of stirring speed on the leaching of different metals present in NiMH battery material was studied using 2 M H_2SO_4 at 348 K, 100 g/L pulp density for 120 min. The recovery of all metals was almost constant

irrespective of the stirring speed beyond 300 rpm (data not included here). In order to keep entire range of particles under suspension a constant stirring speed of 500 rpm was maintained during the leaching experiments which was found to be sufficient to minimize the diffusion layer of lixiviant around the battery powder being leached out.

4.1.4 *Effect of pulp density:* The effect of pulp density (25 - 150 g/L) on the leaching of the metals was studied in 2 M H_2SO_4 at 348 K and 120 min. Results given in Fig. 4.3 clearly show that the leaching efficiency of all the metals decreased as the pulp density increased. These data also infer that the dissolution of the metals is nearly constant in the pulp density range of 20 -100 g/L. In particular, 92.9% Ni, 98.1% Co, 68.4% Fe, 96.7% Mn and 99.2% Zn were recovered at 20 g/L pulp density. Increasing the pulp density to 100 g/L adversely affected the metal dissolution. The leaching efficiency of Ni, Co, Fe, Mn, Zn was found to be 91.6, 97.8, 65.5, 93.5 and 99.2% Zn respectively at 100 g/L pulp density. Hence 100 g/L pulp density can be taken as optimum for rest of the experiments.

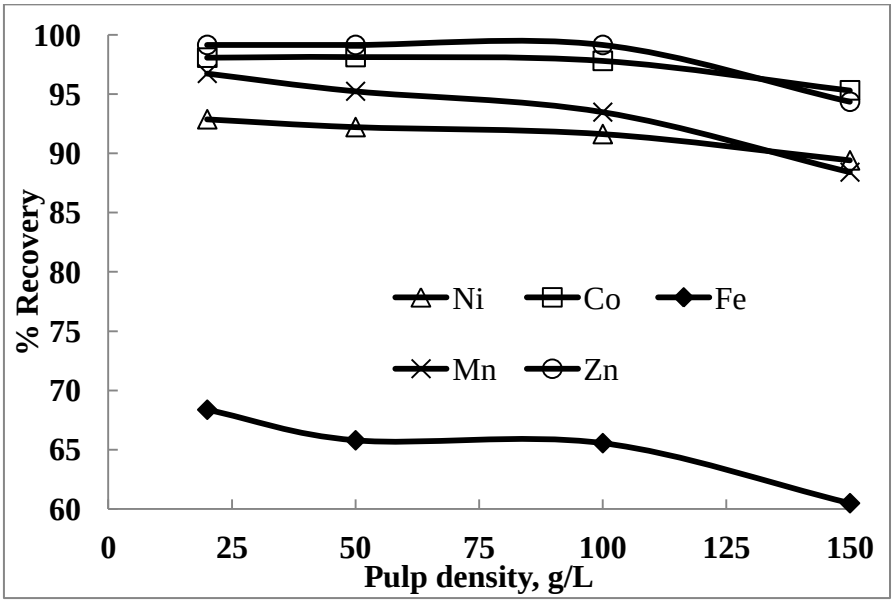

Fig. 4.3: Effect of pulp density on the leaching efficiency of spent Ni-MH battery powder [Acid: 2 M H_2SO_4, t: 120 min., T: 348 K]

4.1.5 *Effect of temperature:* The effect of temperature (from 305 to 348 K) on the dissolution of metals present in the spent batteries in 2 M H_2SO_4 was examined while maintaining other leaching parameters mentioned above. Results presented

in Fig. 4.4 show that 72.3% Ni, 89.9% Co, 50.3% Fe, 73.2% Mn and 89.1% Zn can be leached out at room temperature (305 K) in 120 min. The leaching efficiency of the metals increased with the increase in temperature. Thus at 348 K, the recovery of Ni, Co, Fe, Mn, and Zn was found to be 91.6, 97.8, 65.5, 93.5 and 99.2%, respectively when the battery powder was leached for 120 min. Effect of varying the temperature with time on the leaching of metals is illustrated in Fig. 4.5(a-e). The leaching efficiency has steadily increased till 120 min and thereafter it changed only slightly. These data obtained with time and temperature can be utilized to understand the rate of leaching while applying the standard kinetic rate expressions.

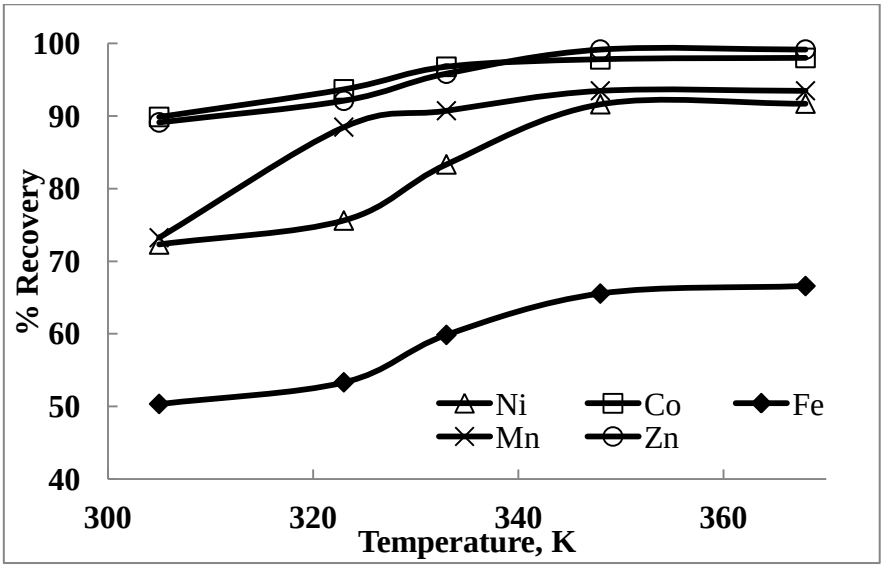

Fig. 4.4: Effect of temperature on the leaching efficiency of spent Ni-MH battery powder [Acid: 2 M H_2SO_4, t: 120 min., S/L= 100 g/L]

4.1.6 *Kinetics of Leaching:* The leaching pattern of each metal at varying temperatures with time was examined using the standard shrinking core models. The leaching results from this study over the first 120 min show the best fit to the surface chemical control model [$1-(1-x)^{1/3} = k_c.t$ --- Eq. 1.17, Chapter 1] as depicted in Figure 4.6 (a-e) when [$1-(1-x)^{1/3}$] verses t was plotted for the metals such as Ni, Co, Fe, Mn and Zn. This is also evident from the high R^2 values (> 0.97) as shown in Table 4.1. A separate plot was also made for all the rare earth metals together as REs and in this case also the chemical control model was found to be applicable; details are included in section 4.2. Table 4.1 also lists the values of apparent rate constants for all the metals with their equivalent correlation

coefficients. The kinetic data show poor fit to the diffusion control model [1-(2/3)x-(1-x)$^{2/3}$ = k_d.t -- Eq. 1.18, Chapter 1] (Fig. 4.7) owing to low values of correlation coefficient (0.92-0.96).

The values of the apparent rate constants (k_c) obtained from the kinetic plots for each metal were used for the construction of Arrhenius plots (ln k_c vs. 1/T) as depicted in Fig. 4.8. The calculated activation energy (E_a) values acquired during the leaching of the base metals viz., Ni, Co, Fe, Mn and Zn have been found to be 8.7, 6.8, 7.12, 6.7 and 7.9 kJ /mol, respectively in the temperature range 305-348 K. From Table 4.1 and Fig. 4.8, it is concluded that the reaction kinetics adhere to the chemical controlled mechanism. Although, the low values of activation energy might suggest that the acid leaching of the metals from the spent batteries follows other mechanism which includes diffusion or mixed control models. However, it appears that the rate controlling mechanism of heterogeneous dissolution reactions in the present system (Eqs. 4.1-4.3) can be better explained from the plots of the kinetic equation represented by chemical control model and corresponding correlation coefficients rather than that of the activation energy values (Olanipekun, 1999). The chemical control model can be further validated by examining the change in surface morphology through the SEM studies before and after the leaching.

4.1.7 *Characterization of solids and leaching mechanism:* The electrode powder of the spent batteries was characterized by XRD and SEM-EDAX before and after the acid leaching. As mentioned in section 2.1, the XRD of the untreated powder reflects the presence of nickel bearing phases in major amounts ($Ni(OH)_2$, Ni, Nd_2Ni_7, Ni_5La) whereas the minor phases being $CeCo_3$, Sm_2Fe_{17} and Ce_2Ni_7. Upon treatment with 2 M H_2SO_4 at 348 K over 30 min, the major phases (Table 4.2) were identified to be Ni, Mn_2O_3 and MnO_2. More details including the XRD patterns and the phases identified along with the JSPDS files are given in the subsequent section (4.2). When the leaching was carried out for 60 min, CoO.NiO was identified to be the major phase, while Mn_2O_3 and Ni being the minor phases. The amount of the residue obtained after 120 min of leaching was so small to collect from the filter paper and hence not analyzed by chemical method nor characterized by other techniques.

Table 4.1: The values of apparent rate constants with their correlation coefficients for leaching of Ni-MH powder at different temperatures

T (K)	Apparent rate constant (Chemical control model) (10^{-3} min^{-1})					Chemical control model					Diffusion control model				
						Correlation Coefficient, R^2					Correlation Coefficient, R^2				
	Ni	Co	Fe	Mn	Zn	Ni	Co	Fe	Mn	Zn	Ni	Co	Fe	Mn	Zn
305	3.02	4.45	1.78	3.69	4.49	0.976	0.994	0.990	0.991	0.982	0.969	0.952	0.961	0.956	0.973
323	3.47	5.07	1.99	4.22	5.11	0.989	0.997	0.994	0.992	0.980	0.952	0.969	0.947	0.950	0.975
333	3.81	5.75	2.22	4.66	5.57	0.986	0.994	0.991	0.987	0.983	0.958	0.974	0.949	0.971	0.975
348	4.66	6.12	2.51	5.08	6.67	0.989	0.990	0.992	0.991	0.986	0.947	0.981	0.944	0.973	0.977

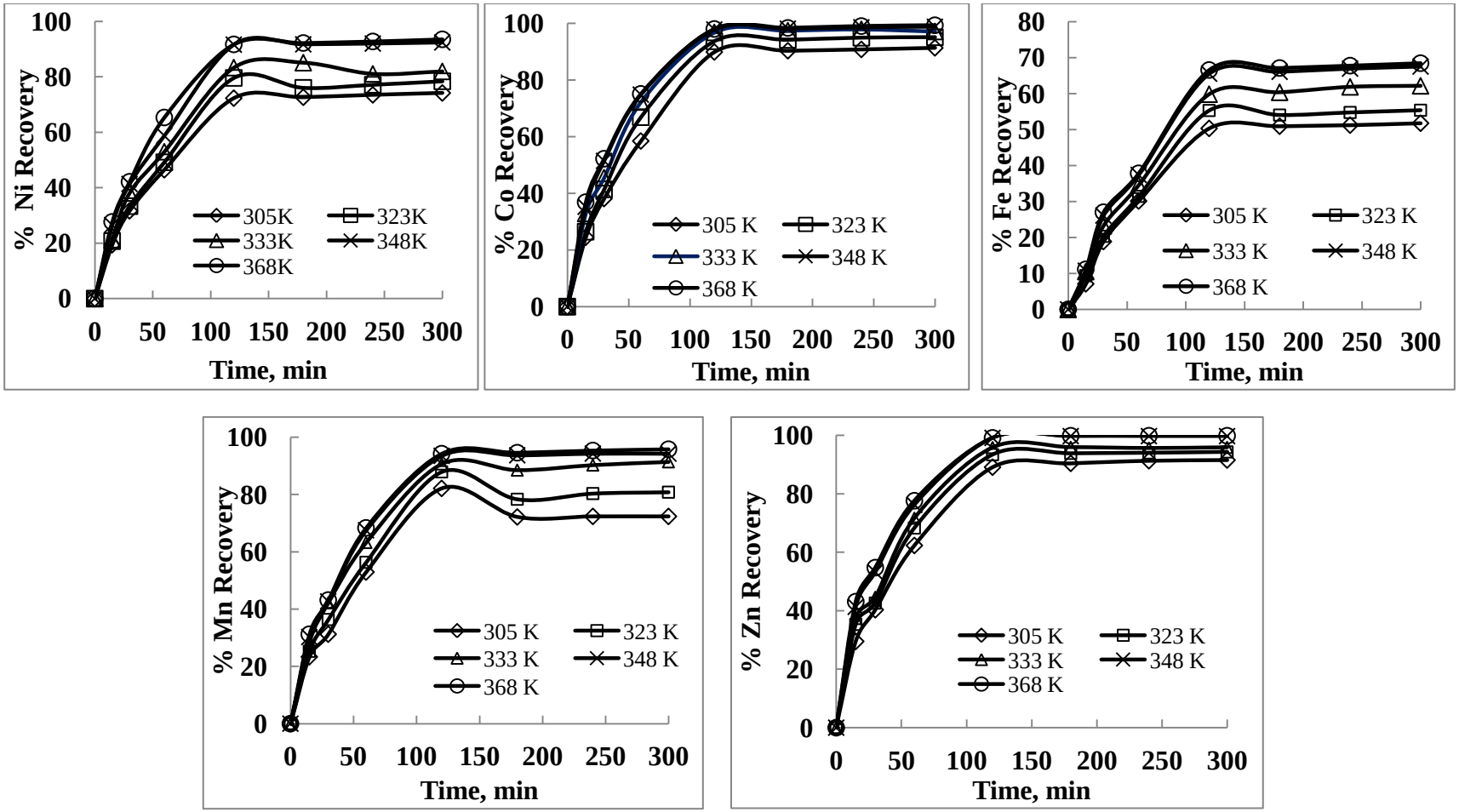

Fig. 4.5: Effect of temperature on the leaching efficiency of different metals from electrode powder at different time intervals [Acid: 2 M H_2SO_4, t: 120 min., S/L =100 g/L]

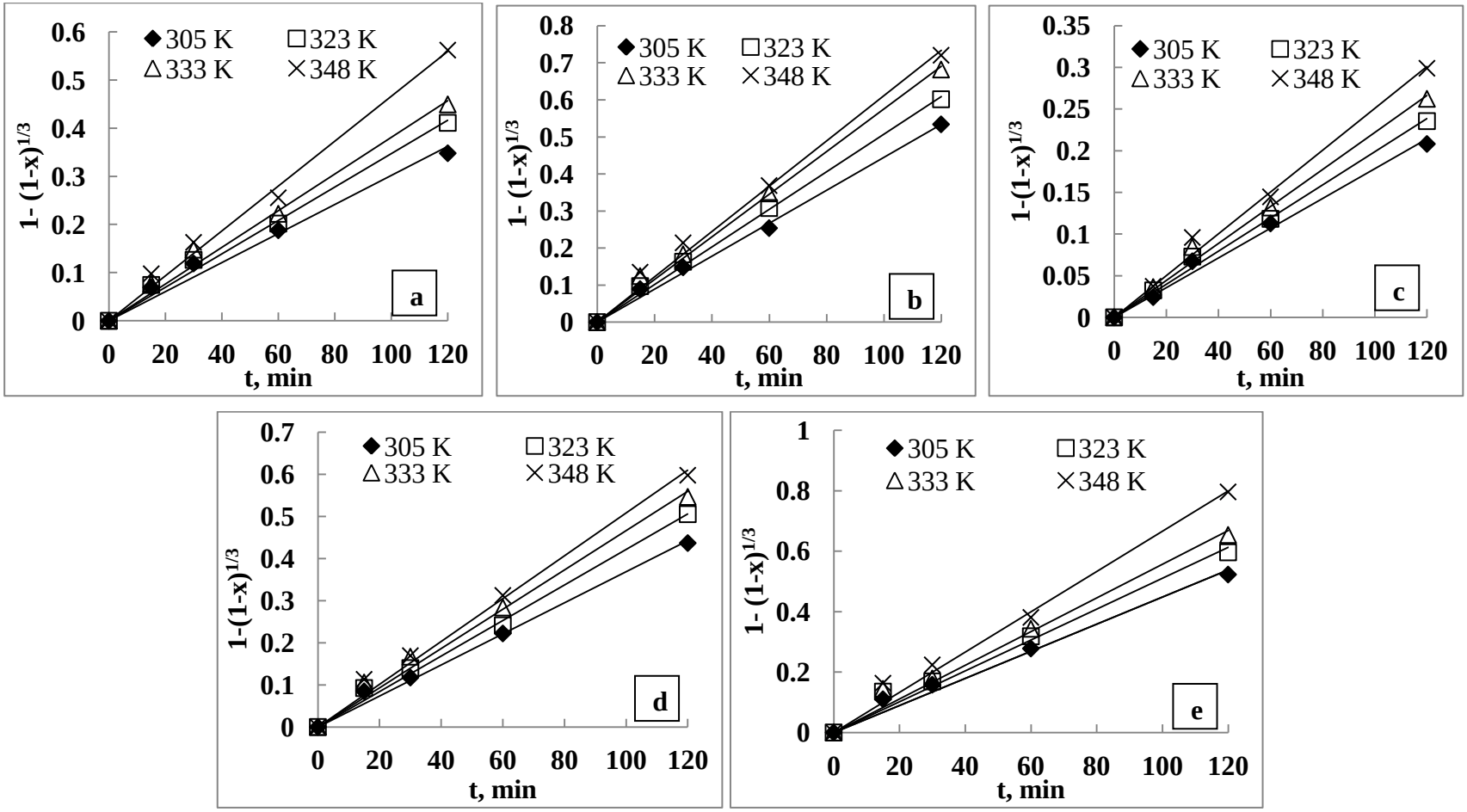

Fig. 4.6: Chemical controlled kinetic model of leaching for (a) nickel (b) cobalt (c) iron (d) manganese and (e) zinc in the temperature range 305-348 K.

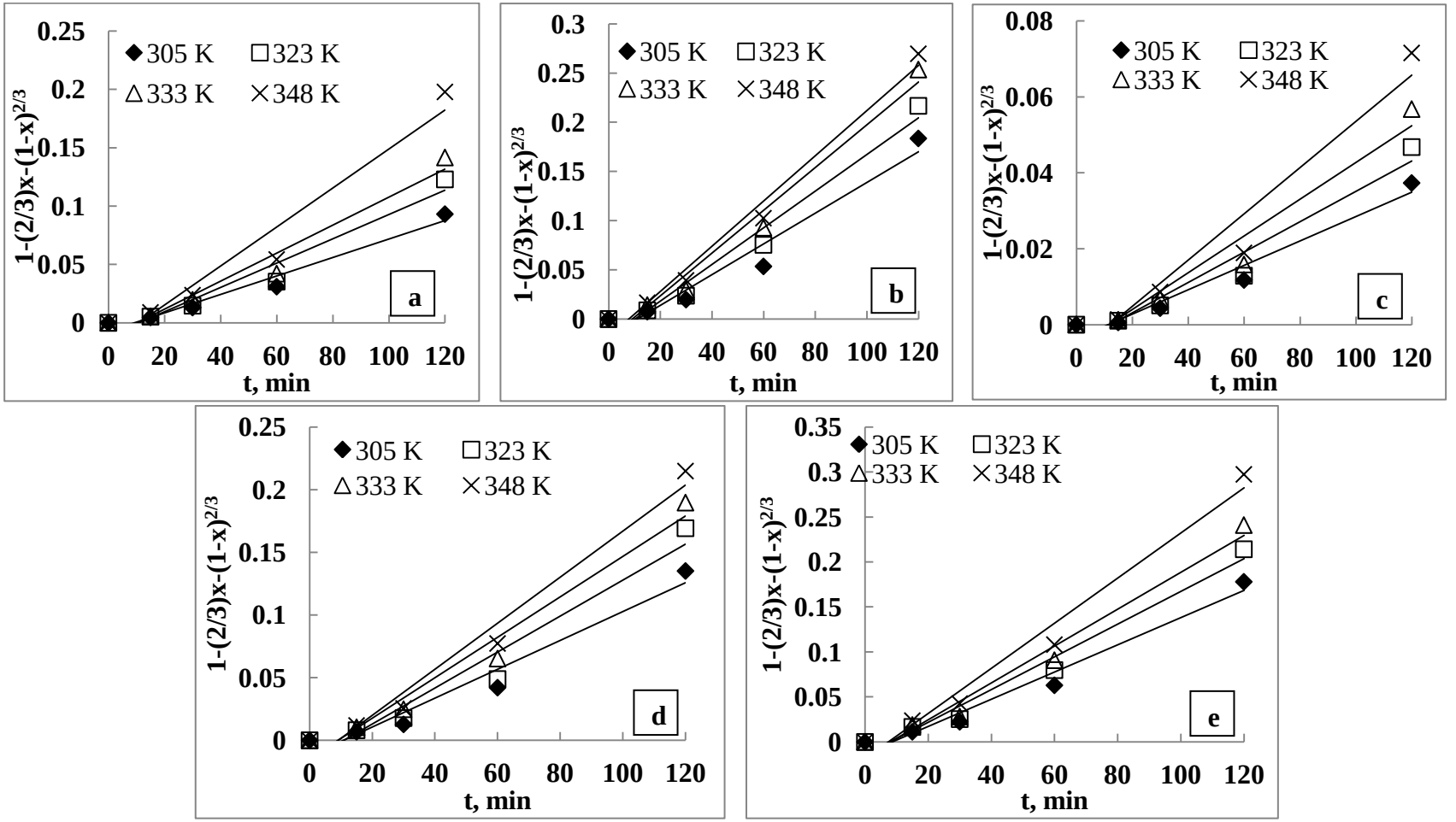

Fig. 4.7: Diffusion controlled kinetic model of leaching for (a) nickel (b) cobalt (c) iron (d) manganese and (e) zinc in the temperature range 305-348 K.

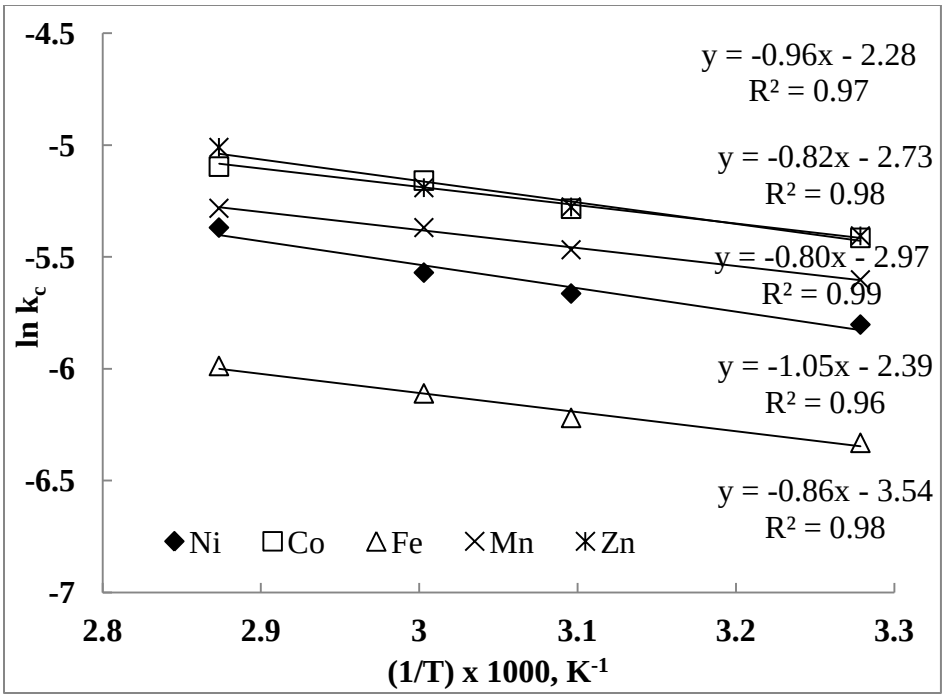

Fig. 4.8: Arrhenius plot for the leaching of the metals from electrode powder in the temperature range 305-348 K

The SEM image of the untreated sample shown in Fig.2.7 (Chapter 2) infers the presence of dispersed metal aggregates with strong intercalation of the nickel based phases (as identified by XRD analysis). Figs. 4.9 and 4.10 show the SEM-EDAX of the residues obtained after 30 min and 60 min of leaching under the optimum conditions including the temperature (348 K). The increased corroded surface of the particles can be observed with the progressive leaching of the electrode material. The morphology of the leach residue of 30 min shows the excessive dissolution of different metals from the electrode powder as compared to that of the untreated sample (Fig. 2.7).

Table 4.2: XRD phase analysis of electrode material and the leach residues at different time intervals. Leaching conditions: 2 M H_2SO_4 at 348 K and S/L= 100 g/L

Sample	Major Phases	Minor Phases
NiMH battery material	$Ni(OH)_2$, Ni, Nd_2Ni_7, Ni_5La	$CeCo_3$, Sm_2Fe_{17}, Ce_2Ni_7
Leach residue in 30 min	Ni, Mn_2O_3, MnO_2	Ni_5La, CoO.NiO
Leach residue in 60 min	CoO.NiO	Mn_2O_3, Ni

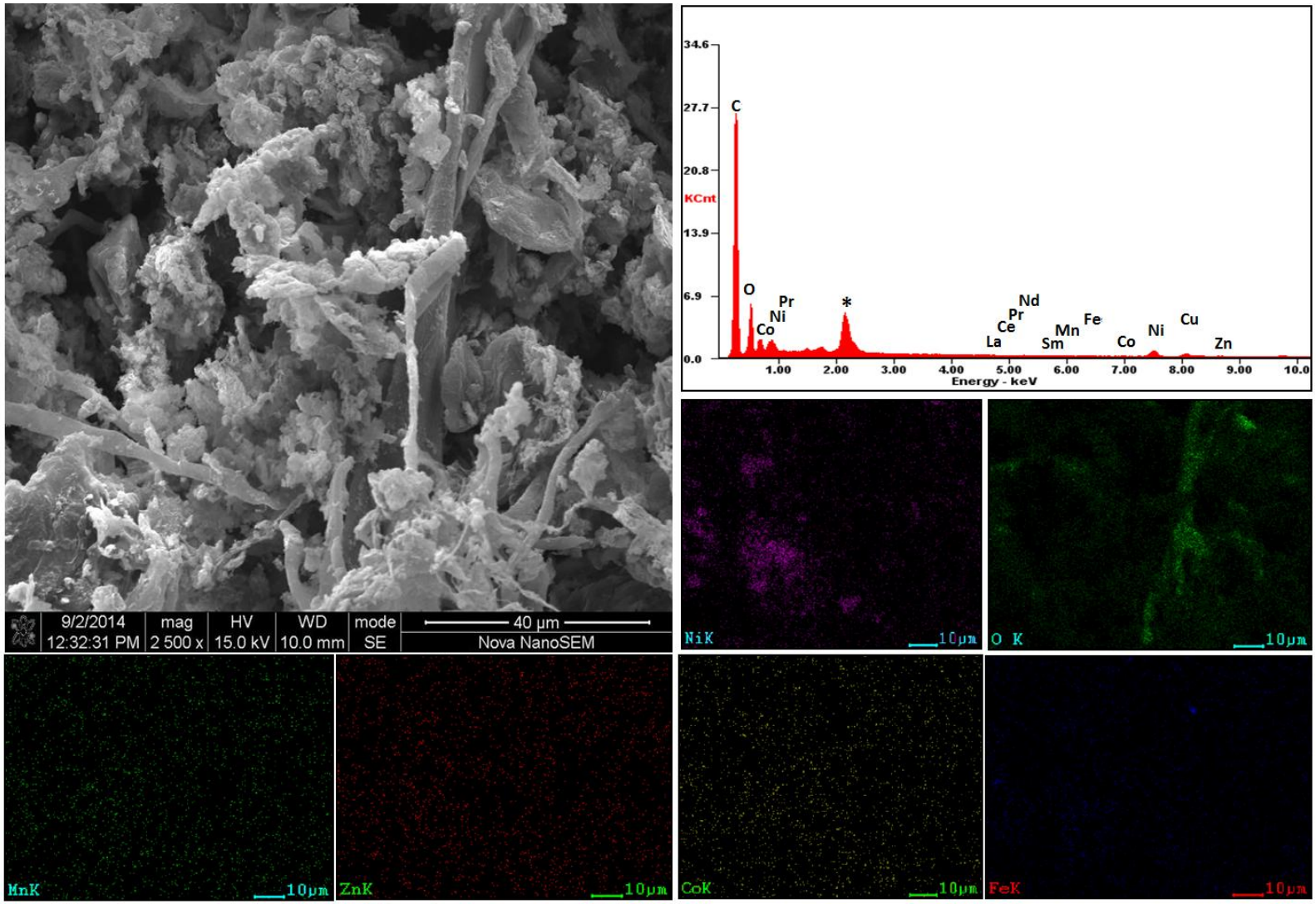

Fig. 4.9: SEM-EDAX analysis of residue at 30 min with the mapping of constituent elements [Leaching conditions: Acid = 2 M H_2SO_4, T = 348 K, S/L = 100 g/L] (* for gold coating)

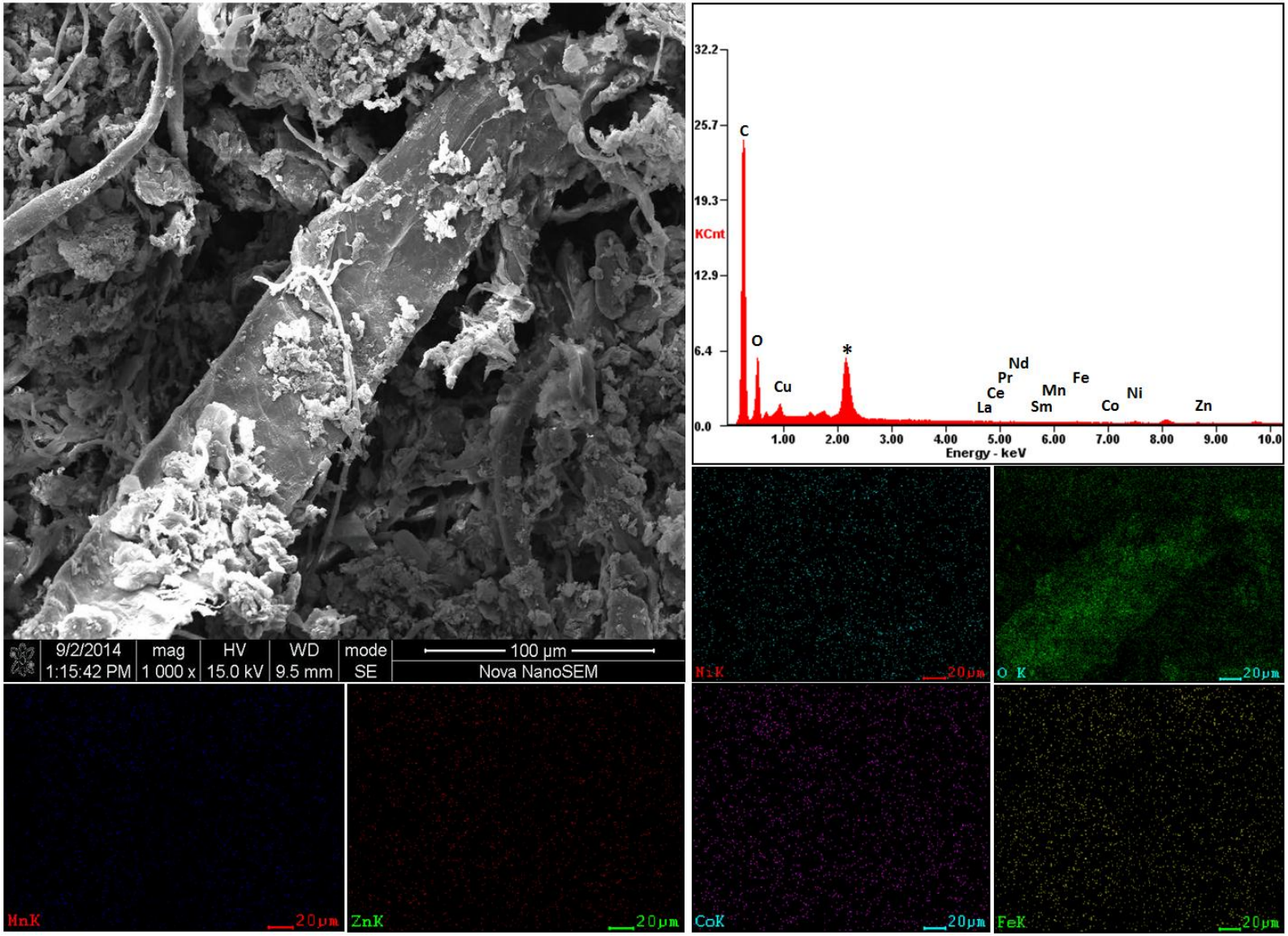

Fig. 4.10: SEM-EDAX analysis of the residue at 60 min of leaching with the mapping of constituent elements [Leaching conditions: Acid =2 M H_2SO_4, T = 348 K, S/L = 100 g/L] (* for gold coating)

The surface of the leached residue looks more like the skeleton of the un-dissolved phases of Ni metal and manganese oxides as given in Table 4.2. This is clearly reflected by the reduction in the metal contents particularly that of nickel in the EDAX of the corresponding leach residue. This was further confirmed by the elemental mapping of different metals (Fig. 4.9). Fig. 4.10 exhibits the morphology of the leach residue in 60 min which reflects highly corroded surface due to the reaction of sulfuric acid with the metal containing phases all around. The brighter dendritic structure appears to be that of NiO.CoO phase as shown by the XRD analysis of the residue (Table 4.2). The EDAX of the residue sample at this stage clearly shows the presence of lower metal contents compared to that of 30 min of leaching. The low concentrations of most metals can also be seen in the respective elemental mapping (Fig. 4.10). Interestingly, the mapping of Fe shows slightly higher level of distribution of this metal as compared to other phases. This may be attributed to the lower recovery of iron (~37% in 60 min and 65.5% in 120 min at 348 K) from the Sm-Fe alloy phase (Sm_2Fe_{17}) present in the material during the course of leaching (Fig. 4.5) or even the formation of some insoluble iron containing phase, which could not be identified by the XRD analysis.

4.2 Leaching of rare earth metals from spent NiMH batteries

It is important to mention that the leaching of base metals from the battery material is accompanied by the simultaneous dissolution of rare earth metals as well. In the previous section (4.1.7) the leaching of rare earth metals together as a group was noted, however, the kinetic aspects as a group are given here in the relevant section. Since the chemical reaction of each RE would differ during the acid leaching depending upon their size (light and heavy REs) and association with the base metals, it is considered worthwhile to dwell upon the effective methodology to recover each REM particularly Nd, Sm, Pr, La and Ce from the spent NiMH batteries. While optimizing the parameters such as acid concentration, leaching time, temperature, pulp density, etc., the kinetics of leaching of the individual rare earth from the spent batteries are also determined. Besides, the reaction mechanism is established by characterizing the leach residues using XRD phase analysis and SEM-EDAX studies.

4.2.1 *Effect of initial H_2SO_4 concentration:* The effect of H_2SO_4 concentration (0.5 - 3 M) on the leaching of rare earth metals from the spent NiMH powder was examined at 348 K, 100 g/L pulp density for 120 min (Fig. 4.11). The leaching of the rare earth (RE) phases such as RE_xNi_y of Ni-MH batteries with the acid may be presented as:

$$RE_xNi_y + \left(\frac{3x}{2} + y\right) H_2SO_4 \rightarrow yNiSO_4 + \frac{x}{2} RE_2(SO_4)_3 + \left(\frac{3x}{2} + y\right) H_2 \qquad (4.4)$$

As can be seen in Fig. 4.11 the leaching of rare earth metals increased gradually with an increase in the acid concentration till 2 M H_2SO_4. With further increase in the acid concentration the leaching efficiency of all the REMs remained almost constant. Hence the optimum acid concentration required for the leaching may be taken as 2 M for further experiments. With 2 M H_2SO_4 about 98% Nd and Sm, 95.5% Pr, 89.4% Ce and 69.5% La were leached out in 120 min.

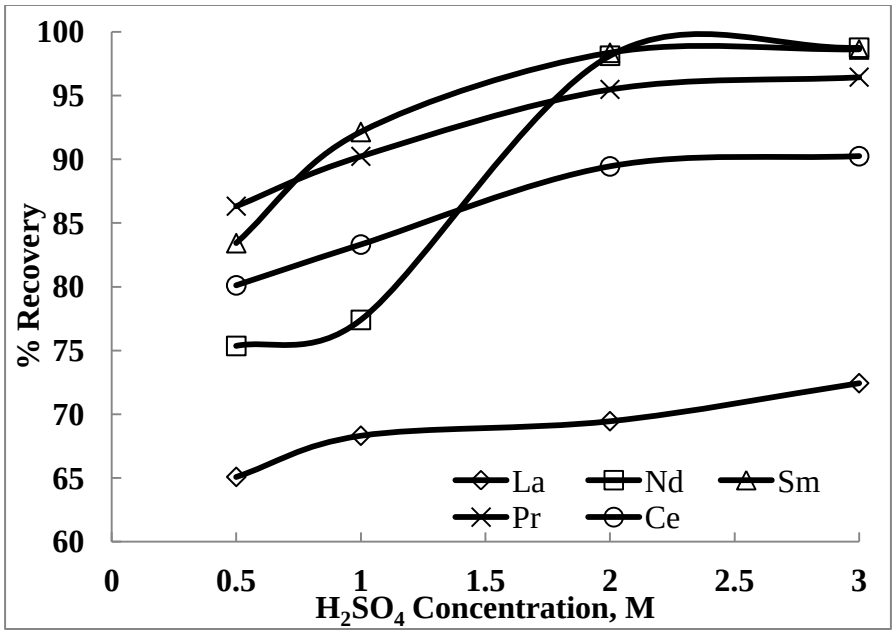

Fig. 4.11: Effect of acid concentration on the leaching of REMs from spent battery powder [T: 348 K, t: 120 min, pulp density: 100 g/L].

4.2.2 *Effect of leaching time:* On optimizing the concentration of acid, the effect of time on the leaching of rare earths was examined at 348 K and 100 g/L pulp density. Fig. 4.12 apparently reflects the increase in recovery of the rare earths with the increase in the leaching time. Leaching efficiency in 60 min was found to be 68.1% for La, 88.3% for Nd, 82.8% for Sm, 76.4% for Pr and 80% for Ce. The dissolution of the REMs was found to be maximum in 120 min and 69.5% La, 98.1% Nd, 98.4% Sm, 95.5% Pr and 89.4% Ce were leached out which may be considered the optimum duration of leaching. The lower leaching efficiency of light REs (La and Pr) may be attributed to the low solubility of their sulfates at the higher temperature, 348 K in this case (Kim and Osseo-Asare, 2012).

4.2.3 *Effect of pulp density:* The effect of pulp density under the conditions of Fig. 4.3 (25-150 g/L) on the leaching efficiency of the REMs was studied (Fig. 4.13). As noticed for base metals the leaching efficiency of REMs was also high at low pulp density due to the presence of sufficient amount of acid to react with the metals; whereas at the higher pulp density, insufficient acidic lixiviant increased the viscosity of the slurry which resulted in decreased mass transfer effect and low dissolution of the REMs in the solution. At 100 g/L pulp density with 2 M H_2SO_4 the maximum

extraction yield obtained was 69.5% La, 98.1% Nd, 98.4% Sm, 95.5% Pr and 89.4% Ce in 120 min. With an increase in the pulp density to 150 g/L, the recovery of all the rare earths decreased. Hence, 100 g/L pulp density can be taken as optimum for rest of the experiments.

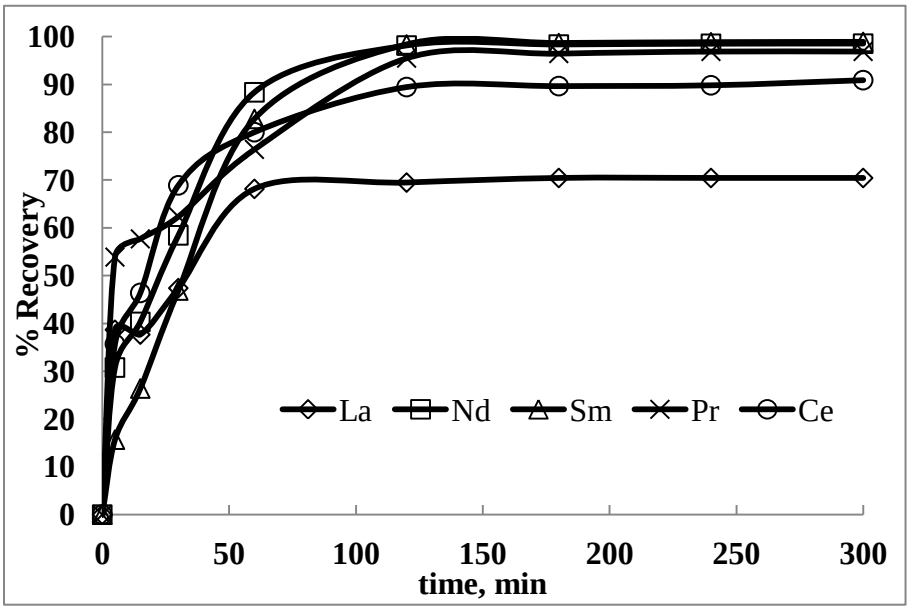

Fig. 4.12: Effect of time on the leaching of metal from the electrode powder of spent batteries.[T: 348 K, acid: 2 M H_2SO_4, pulp density: 100 g/L].

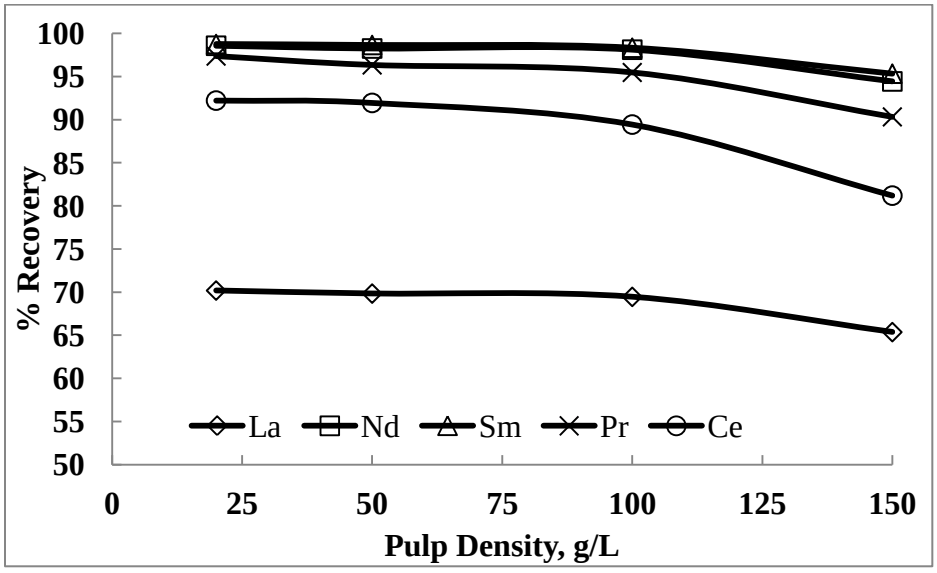

Fig. 4.13: Effect of pulp density on the leaching of metals from the spent Ni-MH battery powder. [Acid: 2 M H_2SO_4, t: 120 min., T: 348 K]

4.2.4 *Effect of temperature:* Effect of temperature (range: 305-368 K) on the dissolution of rare earth metals using 2 M H_2SO_4 can be seen in Fig. 4.14. The percent recovery of all rare earth metals present in the battery powder increased with increase in temperature except for lanthanum. At 305 K (room temperature), 91.5% Nd, 92.1% Sm, 73.3% Pr and 52.1% Ce were leached out which increased to 98.1%, 98.4%, 95.5% and 89.4%, respectively at 348 K.

The dissolution of lanthanum decreased with the increase in temperature beyond 323 K and the maximum lanthanum was leached out (98.1%) at this temperature (323 K). At 348 K, the leaching of lanthanum decreased to 69.5% La in 120 min which may be attributed to the decreased solubility of lanthanum sulfate at higher temperature as mentioned above (Kim and Osseo-Asare, 2012). This is in tune with the lower solubility of light rare earth metal (La and Ce) sulfates in general at the higher temperature. This is further elucidated from the corresponding Eh-pH diagram of the lanthanum at 50 ^oC in presence of other REs relevant to this work (Fig. 4.15). Similar Eh-pH diagrams for Ce in presence of other rare earths are also included in Fig. 4.15 at 25 and 75 ^oC to reflect thermodynamic behavior of this metal. Almost similar result showing low recovery of lanthanum was also obtained during the leaching of lanthanum from the red mud in sulfuric acid (Abhilash et al., 2014). Further increase in the temperature did not show any significant improvement in the leaching of the REMs. Although the leaching efficiency of Ce also exhibit increasing trend with temperature (348 K), its recovery was found to be somewhat lower (89.4%) compared to other metals viz., Sm, Nd and Pr. This lower cerium recovery at the higher temperatures may not be clearly ascribed to the part precipitation of dissolved Ce-sulphate, but can rather be attributed to low dissolution of the associated nickel phase (Ce_2Ni_7) which is evident from the low nickel recovery discussed later (section 4.3).

In order to achieve the best recovery of all the REMs, multiple leaching options could be considered. Thus in stage-I maximum amount of lanthanum can be dissolved at a lower temperature (323 K) followed by II-stage leaching at 348 K to recover all other metals optimally. Nevertheless, 348 K can be chosen as the optimum temperature for the leaching of most rare earth metals.

Effect of varying the temperature with time on the leaching of rare earth metals is shown in Fig. 4.16. The rate of dissolution has steadily increased till 120 min and thereafter it changed only slightly for all metals. Data on the leaching of different rare earth metals can be utilized to examine the kinetics while applying the standard rate equations. However, the kinetics for leaching of lanthanum are ignored as the recovery of La decreased beyond 323 K.

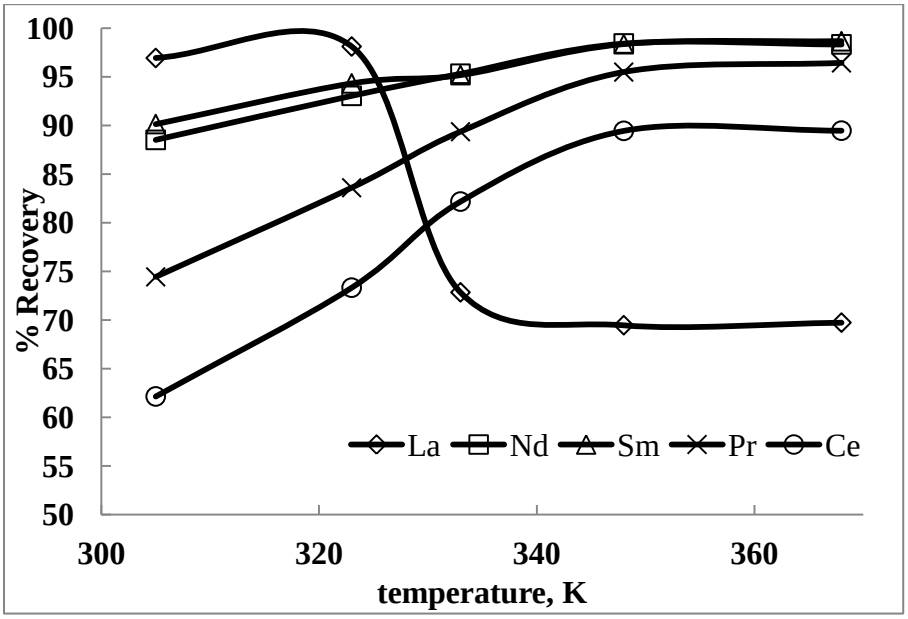

Fig. 4.14: Effect of temperature on the leaching of REMs from spent battery powder. [Acid: 2 M H_2SO_4, t: 120 min., pulp density: 100 g/L]

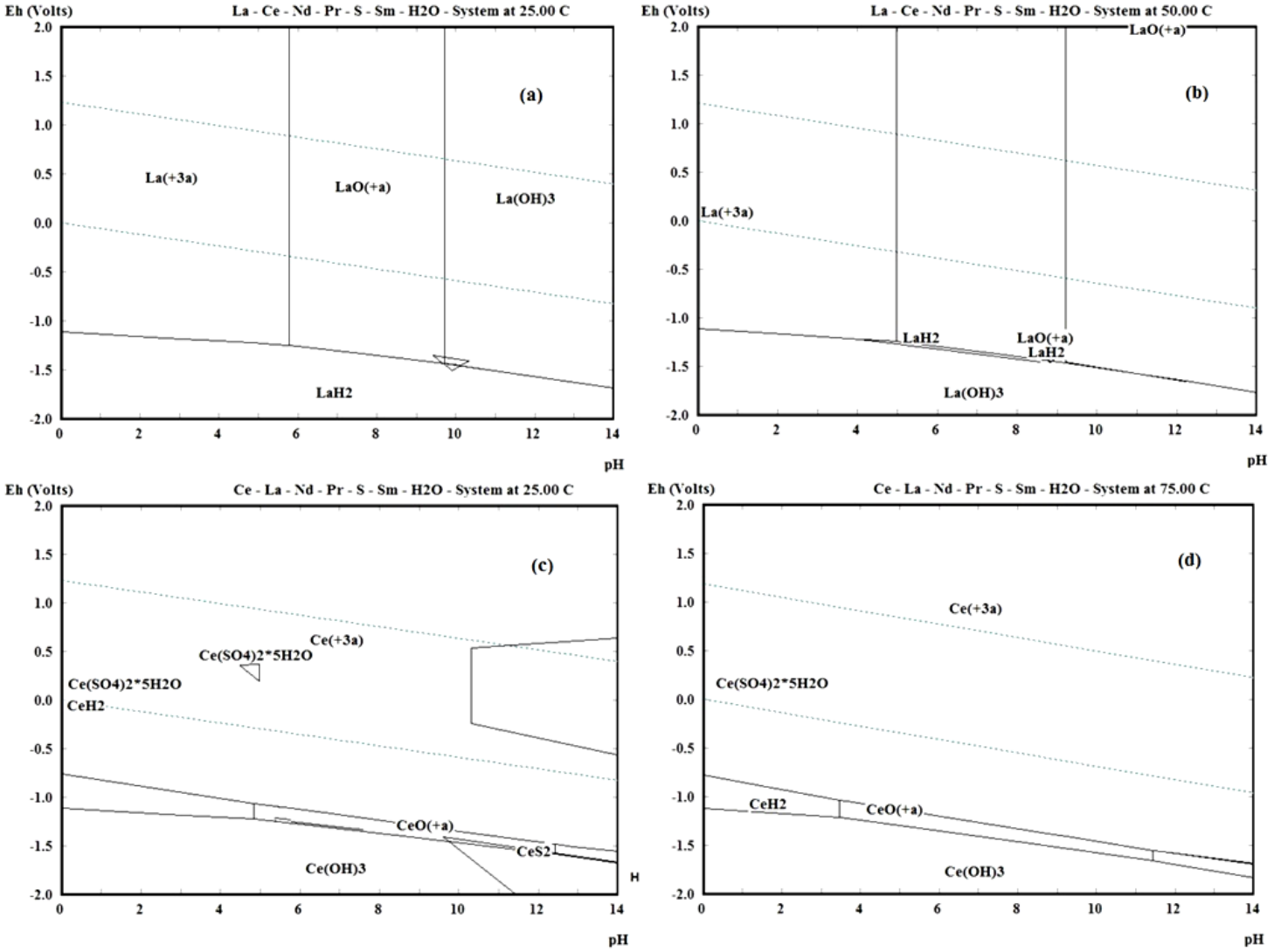

Fig. 4.15: Eh-pH diagram of (a) La-S-H_2O system at 298 K, [La] =0.02 M; (b) La-S-H_2O system at 323 K [La] =0.002 M; (c) Ce-S-H_2O system at 298 K, [Ce] = 0.031 M; (d) Ce-S-H_2O system at 348 K, [Ce] =0.031 M

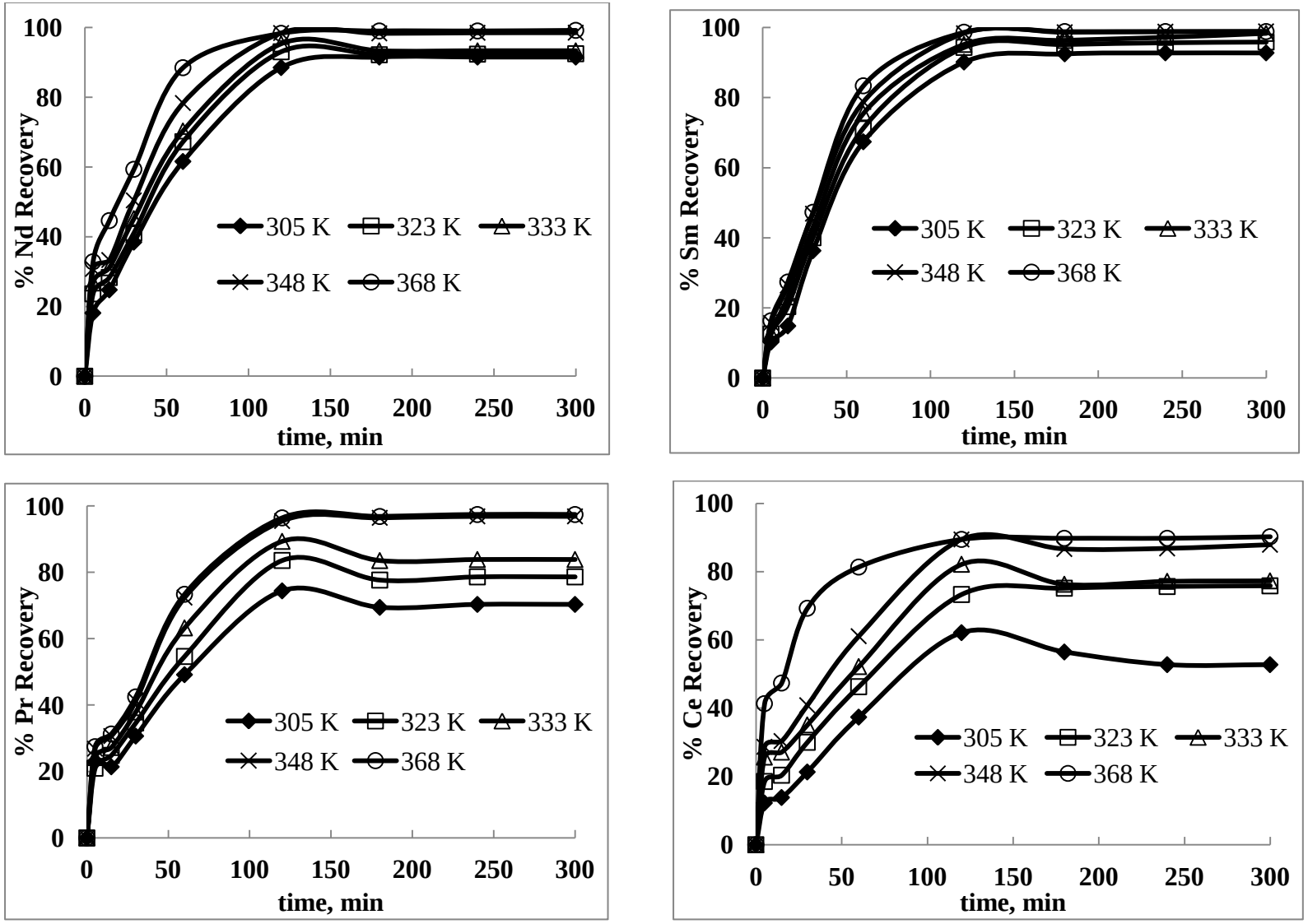

Fig. 4.16: Effect of temperature on the recovery of rare earth metals from NiMH battery powder at different time intervals [Acid: 2 M H_2SO_4, t: 120 min., PD: 100 g/L]

4.2.5 *Kinetics of leaching:*

a. Leaching kinetics of REs together/as a group: Time course data for recovery of all the REs together present in the battery material at different temperatures under the conditions of Figure 4.17a (2 M H_2SO_4, 120 min, 100 g/L pulp density) show good fit to the chemical control shrinking core model as mentioned in section 4.1.7. This is evident from Fig. 4.17b when straight lines are obtained for the plots of $1-(1-x)^{1/3}$ *vs.* t at varying temperatures. The activation energy value calculated from the Arrhenius plot (Fig. 4.17c) is found to be 4.95 kJ /mol in the temperature range 305-348 K.

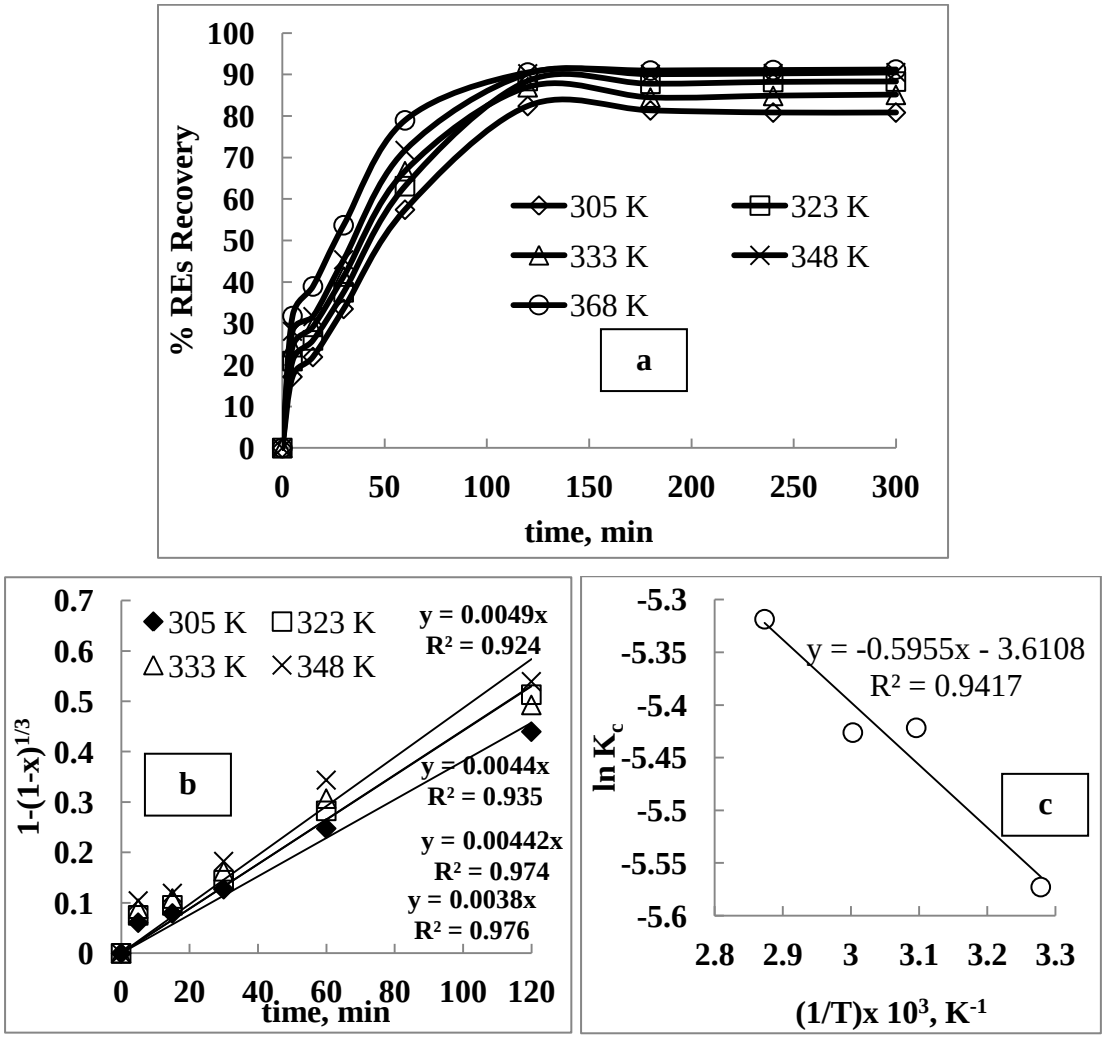

Fig. 4.17: Kinetics of leaching of REs together as a group (a) Effect of temperature (b) Chemical control kinetic model in temperature range 305-348 K (c) Arrhenius plot

b. Leaching kinetics of individual rare earths: In order to obviate the approximation of similar leaching behaviour and consequently the same kinetics for all REs together, the leaching kinetics of individual rare earth metal may be analyzed. For this the kinetic data of Fig. 4.16 can be fitted to the two standard models, the chemical and diffusion control (Eq. 1.17 and 1.19, Chapter 1). The plots of $1-(1-x)^{1/3}$ *vs.* t at different temperatures show (Fig. 4.18 a, b, c, d) that the kinetic data fitted well to the chemical control model which is evident from the high R^2 values (>0.98). This is clearly inferred from the plots (straight lines) obtained for the metals such as Nd, Sm, Pr and Ce at different temperatures (Fig. 4.18 a-d). The kinetic data however, showed poor fit to the diffusion control model (Figure not given for the sake of brevity). From the values of the specific rate constants (k_c) the Arrhenius plots were constructed (Fig. 4.19). The activation energy (E_a) for the dissolution of the metals viz., neodymium, samarium, praseodymium and cerium has been calculated to be 7.6, 6.3, 11.3 and 13.5 kJ /mol, respectively in the temperature range 305-348 K.

The low activation energy values may suggest that the leaching of the REMs follows the diffusion or mixed control models, but it is quite evident that the plots of the kinetic equation are best represented by the chemical control model. The high correlation coefficients ($\geq$ 0.98) for this model (chemical control) rather than the activation energy values aptly explain the rate controlling mechanism of the present heterogeneous dissolution reactions (Olanipekun, 1999).

4.2.6 *Mechanism of the leaching:* As discussed in section 4.1, the leaching mechanism is again established by using the features of XRD phase analysis and SEM-EDAX studies. The XRD patterns of the untreated powder (Fig. 2.6) and the residues generated during the leaching with time [Fig. 4.20 a,b], exhibit the progressive reduction in the intensities of major peaks of the residues. Upon leaching with 2 M H_2SO_4 at 348 K and 100 g/L PD in 30 min (Fig. 4.20a), the major phases were identified to be metallic Ni (JCPDS No. 01-1260) and manganese oxides (Mn_2O_3, JCPDS No. 76-0150; MnO_2, JCPDS No.12-0715) along with $LaNi_5$ (JCPDS No. 17-0126, 42-1191), CoO.NiO (JCPDS No. 03-0971) and SiO_2 (JCPDS No. 82-1576) as the minor phases (Table 4.3). These phases illustrate the concurrent

dissolution of the rare earths and base metals with time. In 60 min of leaching, no rare earths containing phases were identified, substantiating the dissolution of most REs during the process. This residue was however, found to be rich in CoO.NiO and metallic nickel (major phases) along with minor amount of Mn_2O_3, a lower oxide of manganese (Fig. 4.20b). With negligible amount of residue left out in 120 min of leaching, no further XRD and SEM analysis could be performed.

SEM micrograph (Fig. 4.21a) of the untreated powder clearly shows the dispersed metal aggregates with intercalation of nickel based phases whereas Figs. 4.21b and Fig. 4.21c show the SEM images of the residues obtained at different time intervals of leaching. The micrographs of the residues also show a progressive reduction in the particle size and corrosion on the surface of the particles. For an instance, the residue obtained in 30 min (Fig. 4.21b) of leaching exhibits corroded surface along with a thin wire type aggregate rich in nickel (point 1). High leaching of most rare earths with lower recovery of La (47.4% at 348 K in 30 min, Fig. 4.12) is evident from the EDAX analysis at all three points of Fig. 4.21c. Substantial recovery of metals such as Nd, Sm, Pr, Ce and base metals (Ni and Co) can be seen in 60 min of leaching at point 2 (Table 4.4) which is evident from the high degree of corrosion and clear fragmented vents on the surface of particles with the low amount of the REMs left out in the residue (Fig. 4.21c). Thus SEM-EDAX studies and XRD phase analysis corroborate the mechanism of leaching which proceeds through the chemical reaction of lixiviant on the surface of particles.

Table 4.3: XRD phase analysis of the leach residues at different time (Conditions: 2 M H_2SO_4 at 348 K and 100 g/L pulp density).

Sample	Major phase	JCPDS No.	Minor phase	JCPDS No.
Leach residue (30 min)	Ni	01-1260 04-0850	$LaNi_5$	42-1191
	Mn_2O_3	76-0150	CoO.NiO	03-0971
	MnO_2	12-0715	SiO_2	82-1576
Leach residue (60 min)	CoO.NiO	03-0971	Ni	01-1260 04-0850
			Mn_2O_3	02-0909
			MnO_2	12-0715
			SiO_2	82-1576
Precipitate of REs from Leach liquor	$NaSm(SO_4)_2.H_2O$	40-1480	$CeNa(SO_4).H_2O$	70-0597
	$NaNd(SO_4)_2.H_2O$	40-1481	$NaNd(SO_4)_2$	35-1174
			$NaPr(SO_4)_2$	40-1482

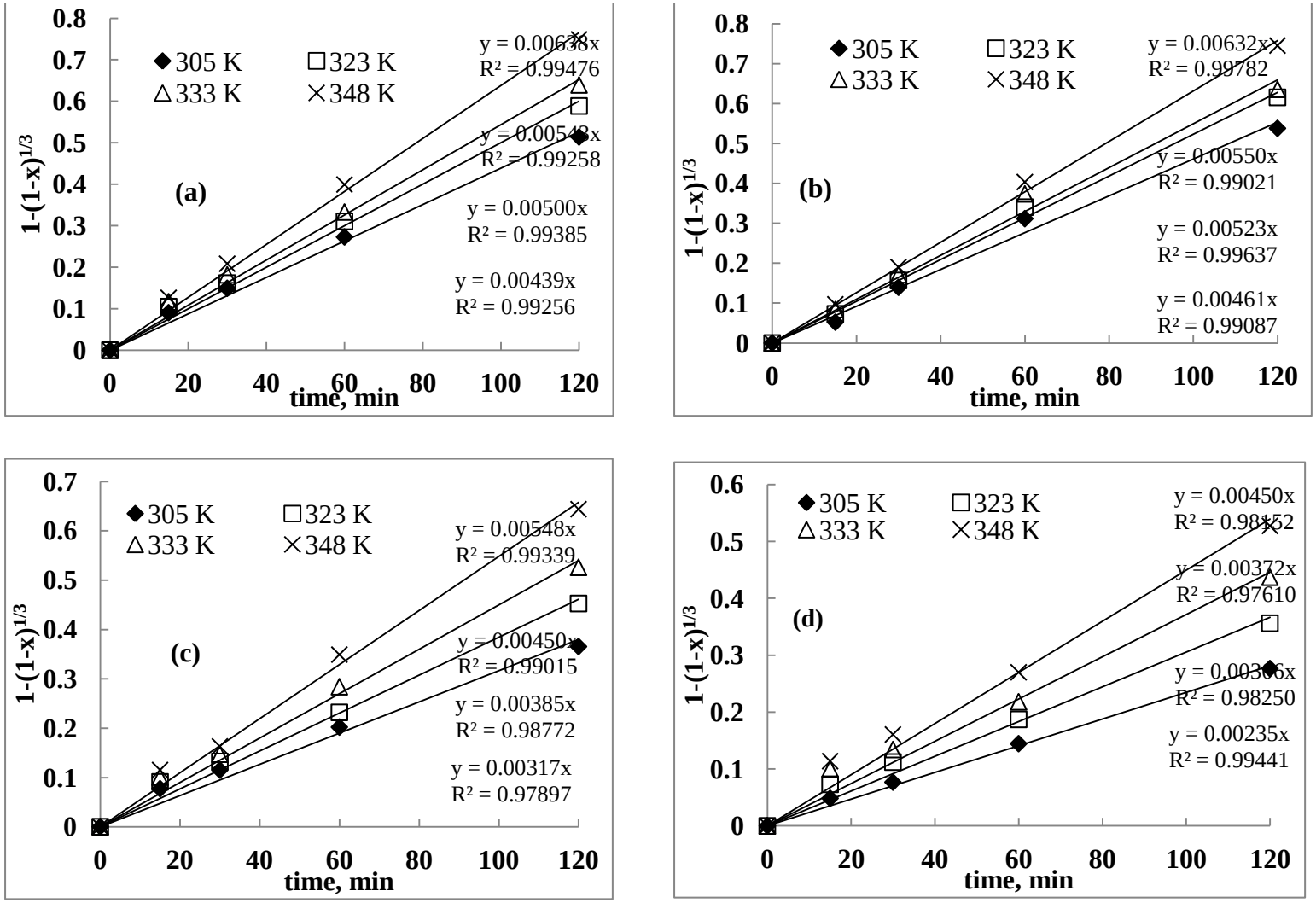

Fig. 4.18: Chemical controlled kinetic model of leaching of (a) Nd (b) Sm (c) Pr and (d) Ce at different temperatures.

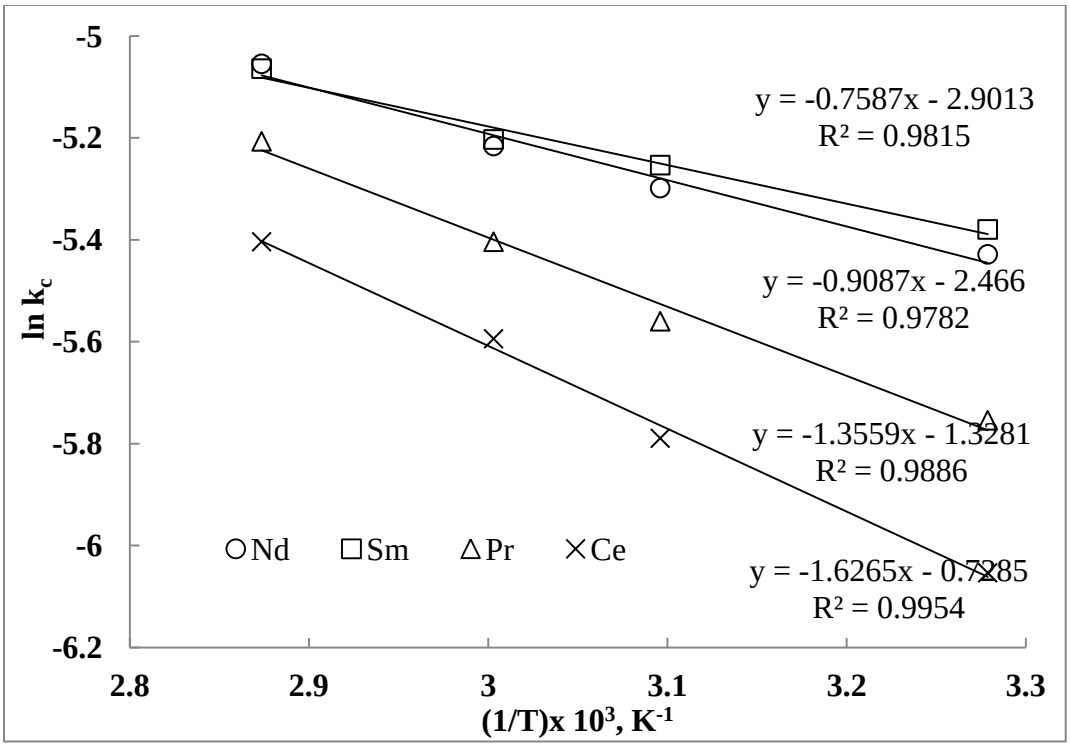

Fig. 4.19: Arrhenius plot for the leaching of the rare earth metals from Ni-MH in the temperature range 305-348 K.

Table 4.4: EDAX analysis of untreated Ni-MH battery powder and the leach residues with time (Acid: 2 M H_2SO_4, 348 K and 100 g/L pulp density).

Elements (wt.%)	Untreated material				Residue at 30 min				Residue at 60 min		
	P-1	P-2	P-3	P-4	P-1	P-2	P-3	P-4	P-1	P-2	P-3
C K	1.82	2.25	5.72	26.05	5.66	82.28	70.64	72.31	63.12	44.21	41.62
O K	24.42	5.90	30.84	30.01	36.49	2.48	13.59	11.09	8.75	30.27	16.71
La L	0	6.14	0.59	0.56	1.04	0.53	1.01	0.45	5.81	0	3.75
Ce L	0.51	0	0	0.26	0.98	0.30	0.90	0.23	3.22	0	0.56
Nd L	0.62	13.78	1.08	0.33	0.92	0.54	1.11	0.73	6.95	0	3.94
Pr L	0.21	2.12	0.12	0	0.86	0.81	0.46	0.29	2.46	0	1.81
Sm L	0.76	15.82	1.79	0	1.28	0.83	1.14	0.93	6.22	0	4.05
Mn K	0.22	0	0.20	0	0.46	0.34	0.56	0.28	2.29	0	1.27
Fe K	0.56	0.57	0.76	0	0	1.34	0	2.30	6.53	0	4.56
Co K	3.00	0.35	4.07	1.27	0.90	1.02	0.55	0.70	5.49	4.97	3.78
Ni K	59.92	53.68	49.08	38.29	15.06	2.82	5.91	3.70	8.85	12.81	10.74
Zn K	8.17	1.53	5.88	3.25	2.54	3.94	2.17	2.16	10.0	16.9	13.72

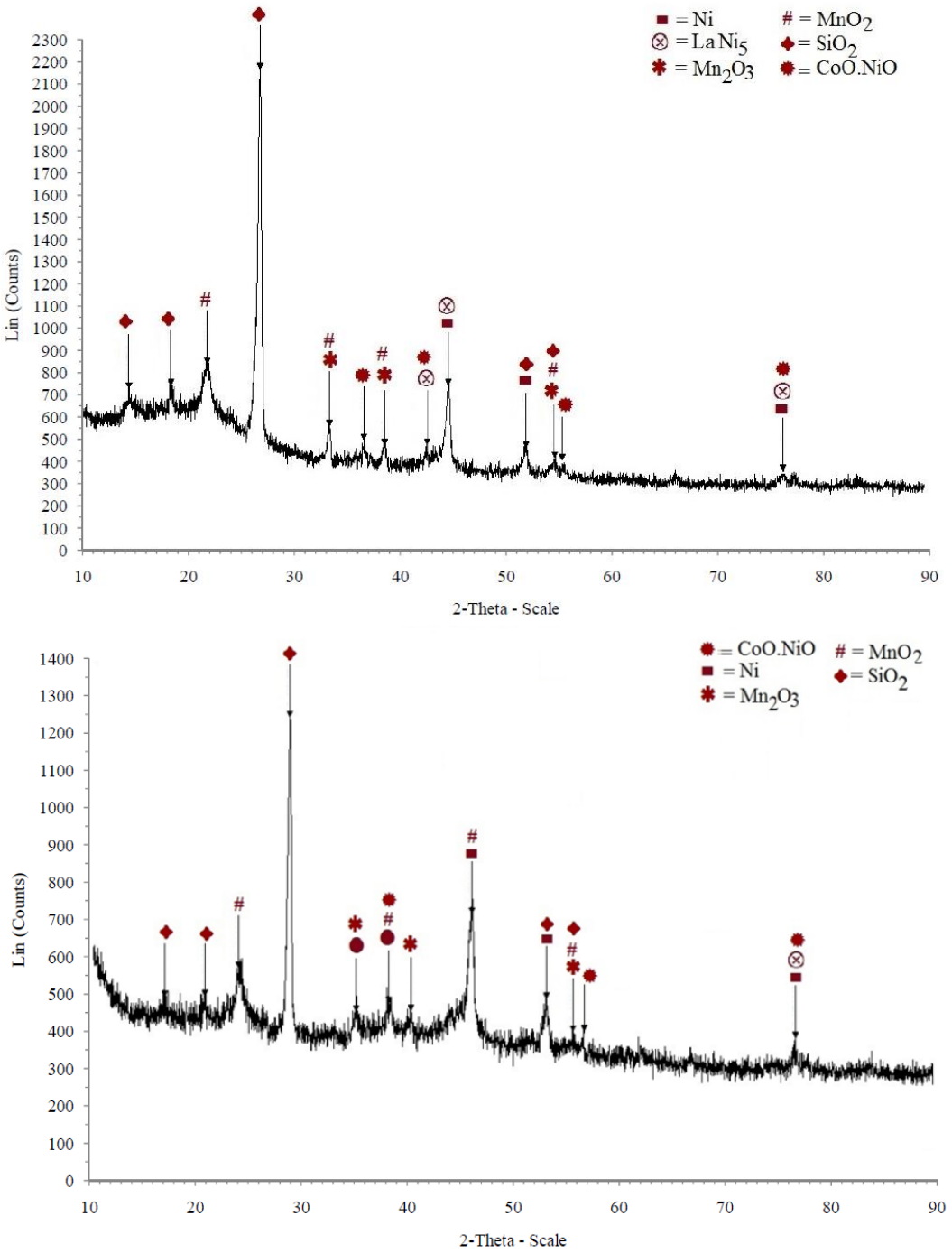

Fig. 4.20: XRD of the (a) leach residue at 30 min; (b) leach residue at 60 min [Acid: 2 M H_2SO_4, T=348 K, PD: 100 g/L]

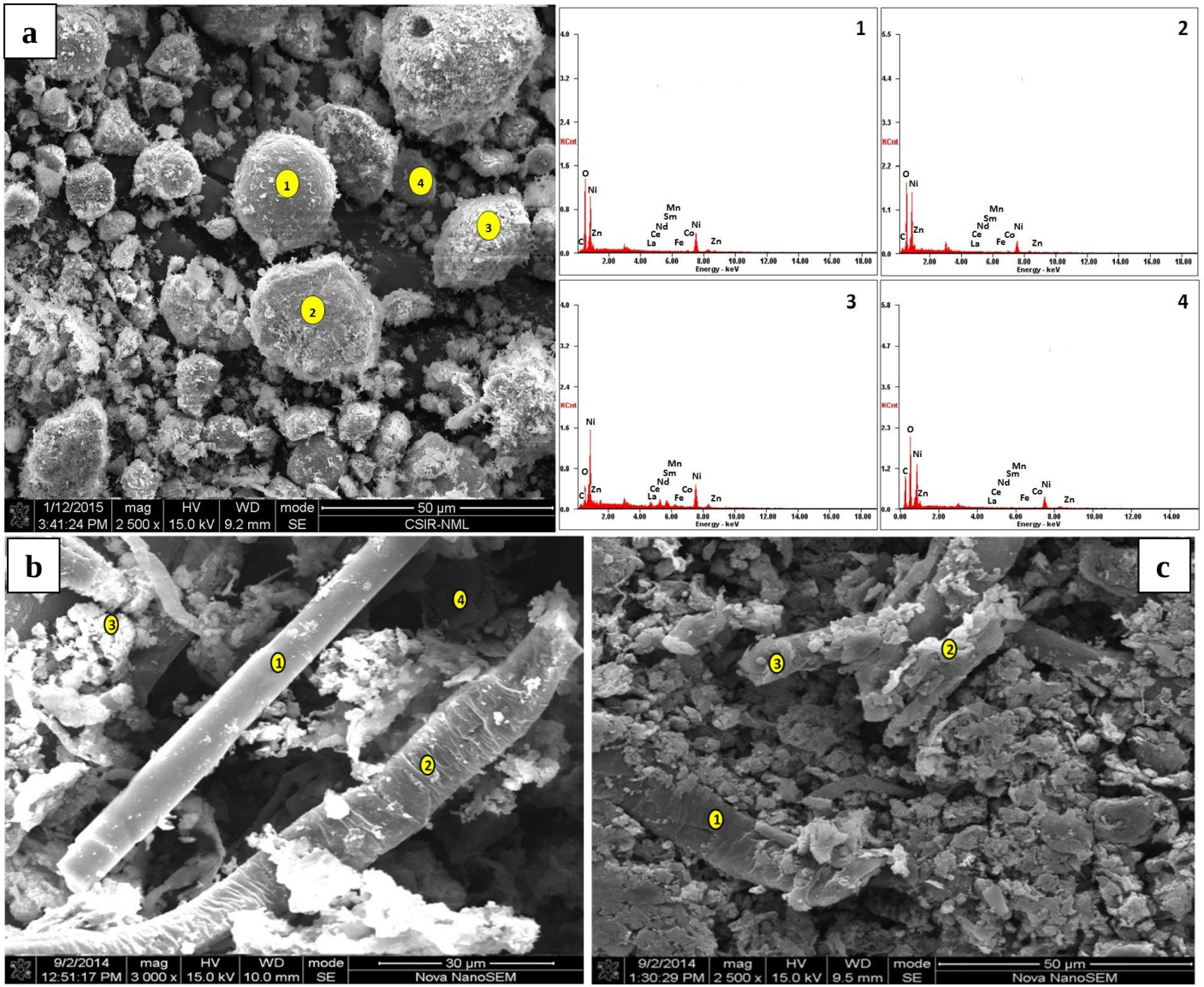

Fig. 4.21: SEM-EDAX of the electrode powder sample (a); residue in 30 min (b) and residue in 60 min (c) [Acid: 2 M H_2SO_4, T=348K, PD: 100 g/L]

4.2.7 *Precipitation of rare earth metals from the leach liquor:* Having established the leaching parameters, the leach liquor obtained under the optimum conditions was taken for the recovery of rare earth metals by precipitation. The composition of the leach liquor was found to be (g/L): 6.0 Sm, 4.3 Nd, 2.15 Pr, 2.2 Ce and 1.75 La along with 53.0 Ni, 4.45 Co, 2.5 Mn, 1.85 Zn and 1.65 Fe. Rare earth metals were precipitated by adding 3 M NaOH solution to the leach liquor (500 mL). The mixed rare earths were precipitated by adjusting the pH to approximately 1.8. At this pH, the precipitation of ferric hydroxide which precipitates at pH >3.0, can be avoided. REs were precipitated in the form of insoluble double sulfate salts as confirmed by the XRD phase analysis (Fig. 4.22). Thus $NaSm(SO_4)_2.H_2O$ and $NaNd(SO_4)_2.H_2O$ were found to be the major phases along with $CeNa(SO_4).H_2O$, $NaNd(SO_4)_2$ and $NaPr(SO_4)_2$ as the minor phases. The composition of the precipitate was found to be (%): 53.4 Sm, 16.3 Nd, 10.8 Pr, 9.6 Ce and 3.8 La. The precipitate also contained small amounts of base metals as impurities. Fig. 4.23 shows SEM of the mixed rare earth salts exhibiting fully grown hexagonal top shaped (flowery) particles comprising of mostly samarium sulfate. Most particles are 4-5 µm long with a few smaller well structured flower bunch agglomerates of 1-3 µm size. The EDAX analysis of the double sulfate salt shows the presence of all the rare earths present in the solution along with some base metals as impurities.

The solution depleted of the rare earth metals can be processed to separate and recover the base metals such as Ni and Co by using a suitable technique such as solution purification and solvent extraction (Bertoul et al., 2009; Innocenzi and Vegliò, 2012b). A general flow-sheet developed for the extraction and recovery of base and rare earth metals from spent nickel metal hydride batteries is illustrated in Fig. 4.24.

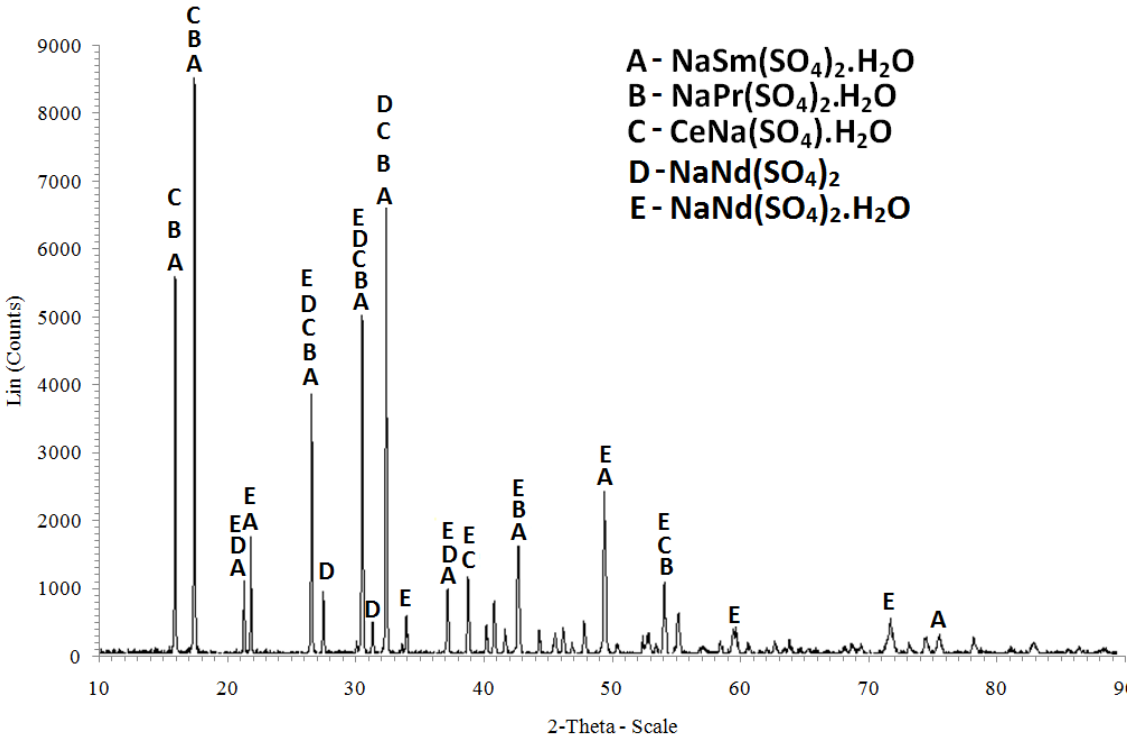

Fig. 4.22: XRD phase analysis of mixed rare earth salts.

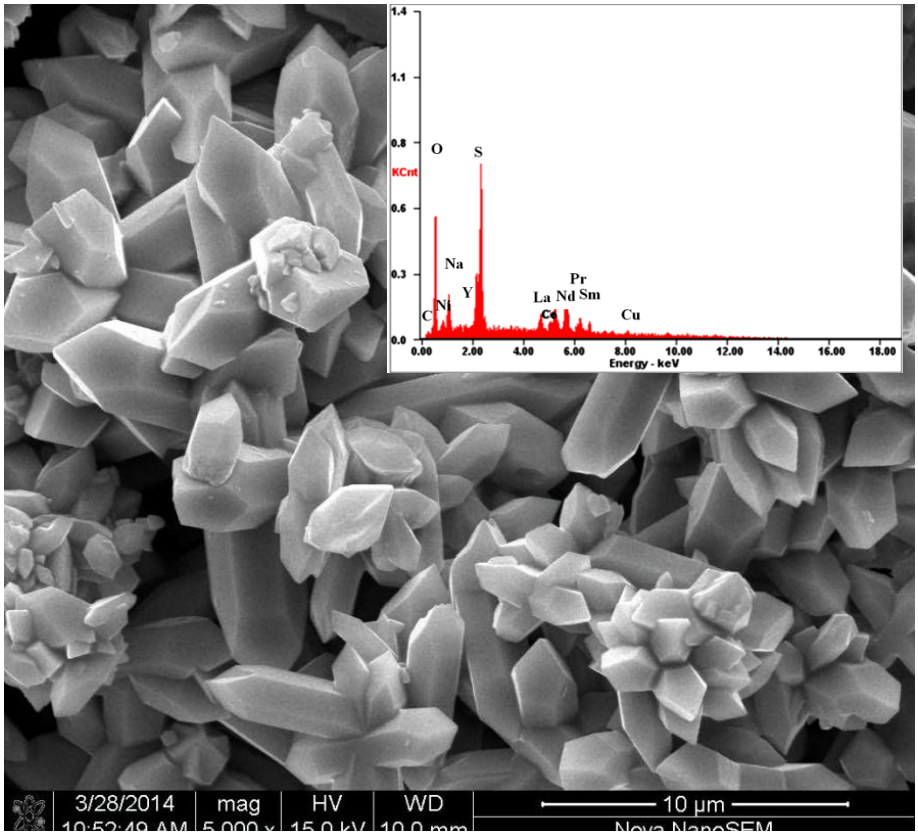

Fig. 4.23: FESEM image of mixed rare earth precipitates at pH~1.8

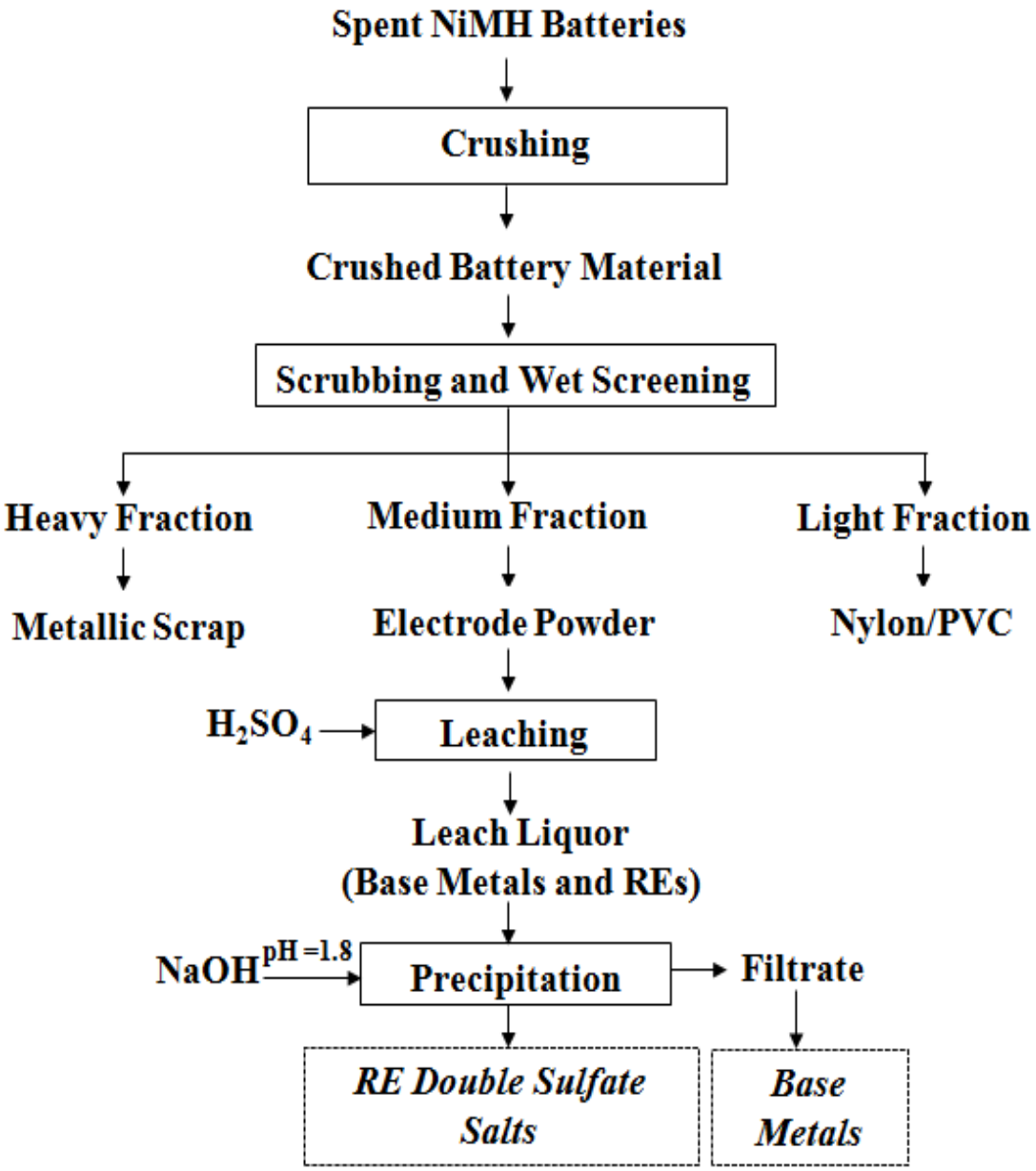

Fig. 4.24: A general flow-sheet developed for extraction and recovery of base and rare earth metals from the spent nickel metal hydride batteries

4.3 Process intensification by acid baking and water leaching to extract metals from the electrode material

The maximum dissolution of nickel, cobalt, iron, manganese and zinc was found to be 91.6, 97.8, 65.5, 93.5 and 99.2%, respectively in a single stage under the optimum conditions comprising of 2 M H_2SO_4, 100 g/L pulp density and 348 K after 120 min of leaching [Section 4.1]. Simultaneous recovery of 98.1% Nd, 98.4% Sm, 95.5% Pr and 89.4% Ce was also achieved under the above conditions [Section 4.2]. As described in Chapter 3 (section 3.4) the sulfation or acid baking process brings about the noticeable change in reactivity of metals to form sulfates thereby breaking the impenetrable layer. This may result in the selective dissolution of some metals of spent NiMH batteries also during the water leaching. The process intensification by acid baking may also exhibit lower acid consumption compared to the direct sulfuric acid leaching. The leaching of all metals directly in H_2SO_4 or sulfuric acid baking-water leaching may follow different mechanisms which need to be investigated. The present study is thus intended to explore the possible selective dissolution of a set of metals over others by sulfuric acid baking-water leaching process. Optimization of various factors affecting the baking of the electrode material, and leaching of different constituents, base and rare earth metals from the baked product is discussed while correlating the phenomenon by the thermodynamic analysis and characterization studies.

4.3.1 *Sulfuric acid baking and water leaching:* Low temperature (100–300 °C) sulfuric acid baking was tested in order to assess the selective leaching of some of the metals over others found in the electrode material. Acid baking transformed the phases of the material which were identified by XRD studies as $NiSO_4$, $(Ni,Fe)SO_4$, NdS_2, Nd_2Ni_7, and $La_{2.607}S_4$ in major amounts. The major and minor phases of the material before and after the baking with the acid at 300 ^oC are listed in Table 4.5.

The baking parameters (amount of sulfuric acid, baking temperature and duration) influencing the dissolution of Ni, Co, Mn, Zn, Fe and REs were optimized. The baked mass was leached with distilled water under a certain conditions unless otherwise stated, to record the solubilization patterns of different metals.

4.3.1.1 *Effect of amount of sulfuric acid*: The amount of sulfuric acid (0.5–3 mL) per 2 g of electrode material for baking affecting the recovery of metals was investigated keeping other conditions constant (baking temperature-300 ^{o}C, time-90 min). The baked material was subjected to water leaching at 75 ^{o}C and 500 rpm for 120 min and results are presented in Fig. 4.25a. As can be seen 1.5 mL H_2SO_4 (0.03 M) is enough to dissolve 91.73% Ni, 94% Zn and 91% REs in 120 min during the water leaching while the dissolution of Co, Fe and Mn was quite poor (23-40%) under this conditions. The pH of the leaching medium remained mostly ~4.8 after 120 min which might have assisted in the dissolution of the highly oxidized sulfates such as that of Ni, Zn and a few REs, leaving only the relatively lesser oxidized phases.

Table 4.5: XRD analysis of spent Ni-MH electrode material before and after processing

Sample	**Major phases**		**Minor Phases**	
	Phases	*JCPDS file No.*	*Phases*	*JCPDS file No.*
Baked electrode material (300 ^{o}C, 2 mL H_2SO_4)	$NiSO_4$	760220	CeS	751991
	$(Ni,Fe)SO_4$	350558	NiSm	190838
	Nd_2S_3	850511	Fe_5Sm	251099
	Nd_2Ni_7	221174	Sm_2O_2S	100230
	$La_{2.607}S_4$	830812	$Nd_2(SO_4)_3$	832244
	$ZnSO_4$	321477	$CoS_{1.97}$	190366
			$MnS_{0.4}O_{2.6}$	210557
Leach-I residue after water leaching (RT, 2 h, 100 g/L PD)	Nd_2Ni_7	221174	Sm_2Co_7	710387
	Mn_2O_3	780390	NiO	731523
			$CoS_{1.97}$	190366
			$Co.O.SO_4$	110305

4.3.1.2 *Effect of baking temperature:* The effect of baking temperature was studied in the range 100-400 ^{o}C for 60 min using 1.5 mL H_2SO_4 (per 2 g material) to examine the dissolution of various metals. Results (Fig. 4.25b) show the rapid increase in leach recovery of Ni, Zn and REs with increase in the baking temperature till 300 ^{o}C and thereafter the leaching efficiency decreases. The recovery of metals from the baked material (at 300 ^{o}C) during the water leaching at 75 ^{o}C in 120 min was recorded to be 91.7 % Ni, 9% Zn and 91% REs, 36.5% Co along with the recovery of ~22% Fe and Mn. Increasing the baking temperature increases the weight to a maximum of ~22%

at 400 ^{o}C as compared to the slight increase in the weight (by ~3%) when the baking temperature is raised from 100 - 300 ^{o}C. This could possibly be due to the increased rate of evaporation of sulfuric acid (boiling point of H_2SO_4: 327 ^{o}C) exceeding the rate of sulfation of metal oxides as discussed in section 3.5 (Chapter 3).

4.3.1.3 *Effect of baking duration*: The effect of baking duration (30-120 min) on the leaching efficiency of metals was investigated by baking the 2 g battery material at 300 ^{o}C with 1.5 mL sulfuric acid. Results shown in Fig. 4.25c indicate that 90 min baking time is sufficient to optimally transform the phases of the spent batteries which can solubilize maximum amount of nickel (91.73%), zinc (94%) and REs (91%) along with lower recovery of other metals (36.5% Co, 22.1% Fe, 23.5% Mn) during the water leaching at 75 ^{o}C in 120 min. Similar trend is observed for the leaching of individual rare earth metal. Fig. 4.25d depicts the maximum recovery of 79% La, 87% Ce and 96-97% Nd, Pr and Sm even from the material baked for 60 min, which remains unaffected after prolonged duration.

Certain phases of Ni, Zn and REs (La, Nd, Ce, Sm, Pr) formed during the baking reaction of electrode powder, can selectively dissolve in water over Co, Mn, Fe and a few REs. Using the thermodynamic data (HSC Chemistry 7.14), the change in the standard free energy can be calculated to predict the feasibility of such reactions. Equations 4.5-4.10 describe the most likely reactions of Ni, Zn, La, Nd with sulfuric acid in the baking process along with the ΔG^{o} at the optimum baking temperature (573 K). The major phases {$Ni(OH)_2$, $LaNi_5$, Nd_2Ni_7, Ni} present in the untreated material may form water soluble sulfates of nickel, zinc and REs during the acid baking while converting Co, Mn, Ce and some Nd to relatively lesser soluble or insoluble sulfides, among others at 573 K (300 ^{o}C).

$$Ni(OH)_2 + H_2SO_{4(l)} = NiSO_4 + 2H_2O \qquad \Delta G^{o}_{573\ K} = -108.6\ kJ \qquad (4.5)$$

$$Ni + 2H_2SO_{4(l)} = NiSO_4 + SO_{2(g)} + 2H_2O \qquad \Delta G^{o}_{573\ K} = -222.4\ kJ \qquad (4.6)$$

$$(Ni, Zn)\ Fe_2O_4 + H_2SO_{4(l)} = (NiFe)SO_4 + ZnSO_4 + 2H_2O \qquad \Delta G^{o}_{573\ K} = -508.7\ kJ \qquad (4.7)$$

$$2.607LaNi_5 + 18.07H_2SO_{4(l)} = 13.035NiSO_4 + 18.07H_2O + La_{2.607}S_4 + 1.035SO_2$$

$$\Delta G^o_{573\,K} = -3143.2\ kJ \quad (4.8)$$

$$Nd_2Ni_7 + 10H_2SO_{4(l)} = 7NiSO_4 + 10H_2O + Nd_2S_3 + O_{2(g)}$$

$$\Delta G^o_{573\,K} = -743.8\ kJ \quad (4.9)$$

$$Nd_2Ni_7 + 20H_2SO_{4(l)} = 7NiSO_4 + 20H_2O + Nd_2(SO_4)_3 + 10SO_{2(g)}$$

$$\Delta G^o_{573\,K} = -2197.6\ kJ \quad (4.10)$$

The high negative values of standard free energy change for Eqs. 4.6-4.10 at 573 K and other temperatures make these reactions thermodynamically feasible in the acid baking process while forming a few metal salts that are potentially leachable in water (**Table 4.6).** This can be further concurred with the residue characterization. Thus the formation of CeS, NiSm, Fe_5Sm, Sm_2O_2S, $CoS_{1.97}$, $MnS_{0.4}O_{2.6}$ is also observed as identified by the XRD phase analysis. The potentially leachable entities of metals such as Ni, Zn and few REs formed in the acid baking step can give rise to their selective dissolution in the first stage (water leach), making the water leached residue rich in Co and Mn, which can subsequently be solubilized in the next stage of leaching. This is in contrast to the selectivity of Co and Li obtained during the baking-water leaching of spent LIBs, since the type of initial phases in the material (NiMH powder) is quite different as that of lithium ion batteries.

Table 4.6: ΔG^o for chemical reactions during baking of cathode active material in temperature range 373-673 K

T (K)	ΔG^o values for the equations 4.5-4.10 (kJ)					
	Eqn 4.5	**Eqn 4.6**	**Eqn 4.7**	**Eqn 4.8**	**Eqn 4.9**	**Eqn 4.10**
373	-95.9	-164.2	-170.6	-3213.974	-782.534	-1658.489
423	-96.2	-170.7	-180.9	-3190.681	-775.031	-1724.164
473	-96.4	-177.2	-195.6	-3167.175	-767.276	-1788.455
523	-96.8	-183.4	-209.6	-3143.788	-759.463	-1851.784
573	-97.5	-189.7	-218.4	-3121.067	-751.903	-1914.816
623	-98.5	-196.1	-226.9	-3100.031	-745.168	-1978.759
673	-99.9	-202.6	-239.3	-3081.602	-739.776	-2044.700

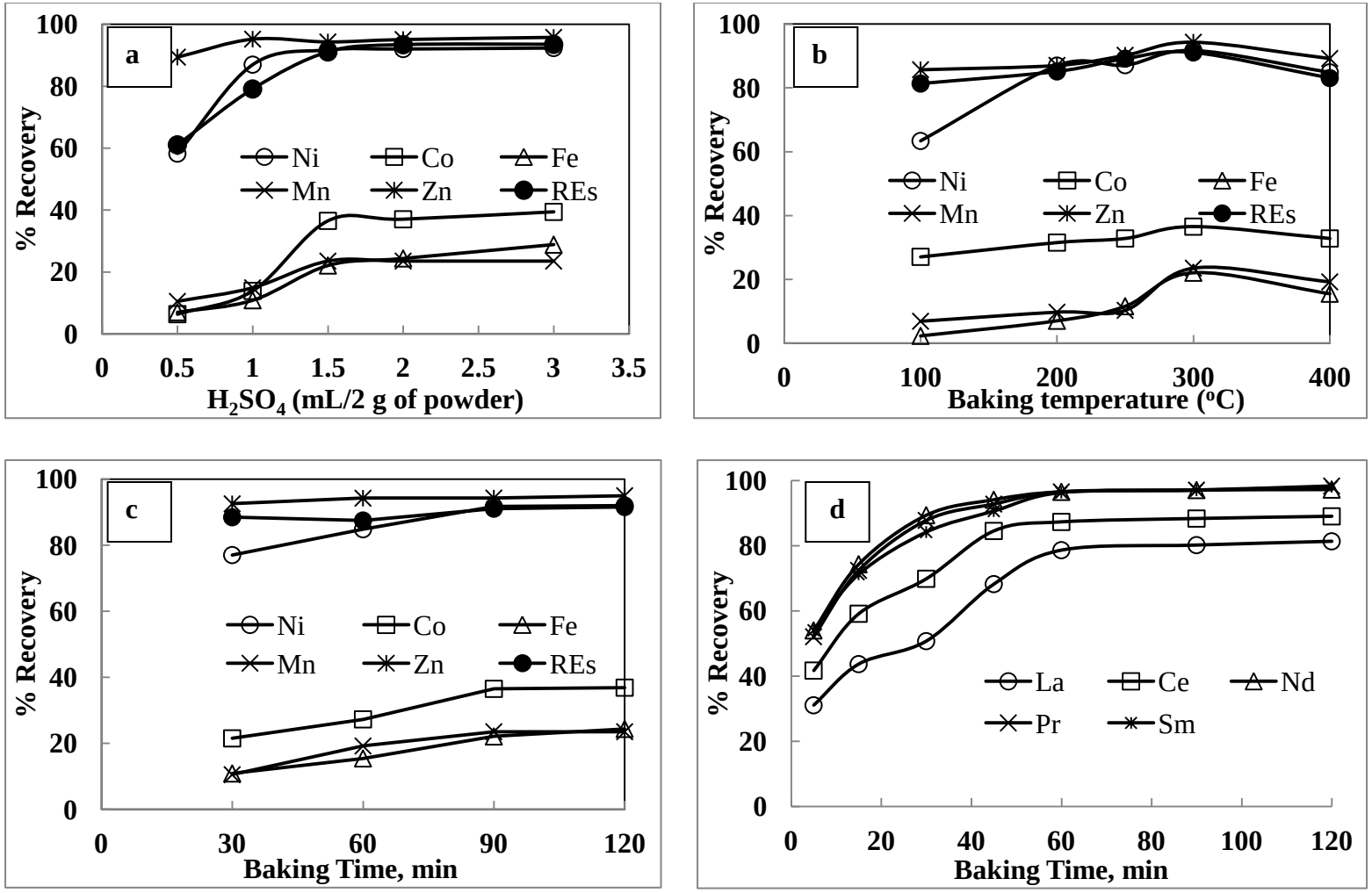

Fig. 4.25: Effect of baking parameters on the recovery of metals in water leaching at 20 g/L PD, 75 ^{o}C in 120 min, (a) amount of sulfuric acid; (b) baking temperature; (c) baking time on all metals; (d) baking time on individual rare earths

4.3.2. *Optimization of the leaching parameters from the acid baked material:* As seen in the previous section, the dissolution of Ni, Zn and REs from the acid baked material is selective in the water leaching stage whereas dissolution of Fe, Mn and Co is much lower. Keeping the optimized conditions of baking while using the same amount of acid (1.5 mL H_2SO_4 per 2 g electrode material) at 300 ^oC for 90 min, leaching parameters like type of lixiviants, time, temperature and pulp density were optimized, and results are discussed below.

4.3.2.1. *Effect of lixiviant type*: In order to examine the dissolution behavior of metals from the baked material, leach experiments were conducted using water and sulfuric acid (1M) as lixiviants, and percentage metal leaching is shown in Table 4.7. As can be seen, water leaching resulted in almost similar level of selectivity for Ni, Zn and REs over iron and manganese, besides lower iron contamination of leach solution, thereby obviating further consumption of an acid or an oxidizing /reducing agent.

Table 4.7: Effect of various lixiviants on the leaching of metals from the baked electrode powder (leaching: 75 ^oC for 120 min, 20 g/L)

Lixiviant used	**% Metal Recovery**					
	Ni	**Co**	**Zn**	**Mn**	**Fe**	**REs**
Water	91.7	36.5	94.3	23.5	22.2	93
1 M H_2SO_4	92.7	37.2	96.5	24.1	28.8	95

4.3.2.2. *Effect of leaching temperature:* Fig. 4.26 (a, b) shows the effect of temperature on the water leaching of metals at 20 g/L pulp density in 120 min. The extraction of all the metals increased steadily with increase in temperature till 75 °C; the leaching efficiency being 91.7% Ni, 94.3% Zn, 36.5% Co, 22.15% Fe, 23.55% Mn (Fig. 4.26a). The recovery of the REs at 75 °C has particularly been high at 96.52% Nd, 96.54% Pr, 96.34% Sm, 87.31% Ce and 78.65% La (Fig. 4.26b). Increasing the temperature further to 95 ^oC has hardly affected the leaching of base and rare earth metals to any significant extent. With a cumulative steady state achieved for all metals at 75 ^oC, this temperature was considered optimum.

4.3.2.3. *Effect of pulp density:* The effect of pulp density on the metal dissolution from the baked material is shown in Fig. 4.27 (a, b). The leaching efficiency of all

base metals decreased slightly with the rise in pulp density above 50 g/L; the dissolution of REs being less affected. At the 50 g/L pulp density, 92.3% Ni, 38.02% Co, 25.1% Mn, 23.7% Fe and 94.6% Zn are recovered in 120 min at 75 ^{o}C (Fig. 4.27a). The recovery of rare earths is recorded to be: 78.7% La, 88.2% Ce, 97.1% Nd, 97.1% Pr and 96.4% Sm (Fig. 4.27b). At the higher pulp density (100 g/L), the recovery of metals decreased to 89% Ni, 36% Co, 21% Fe, 23.5% Mn and 90% Zn, with the lower recovery of REM (85.7%). The higher metal leaching at 50 g/L pulp density can be considered to be optimum for further experiments.

4.3.2.4. *Effect of leaching time:* The baked material is leached with distilled water at 75 °C and 50 g/L PD for different time periods (5-120 min). Improved metal extraction is observed (Fig. 4.28 a, b) with increase in leaching time till 60 min after which only a very marginal increase is noticed. More than 45% Ni, Zn and rare earths were dissolved in 5 min while the dissolution of Co, Fe and Mn was very low (< 2-7%) under this condition (Fig. 4.28a). The selective dissolution of Ni (91.7%), Zn (94.3%) and REs (91%) over Co (36.5%), Fe (22.1%) and Mn (23.5%) is clearly noticed in 60 min of leaching. The recovery of constituent RE was found to be 78.7% La, 87.3% Ce, 96.5% Nd, 96.5% Pr and 96.3% Sm in 60 min (Fig. 4.28b).

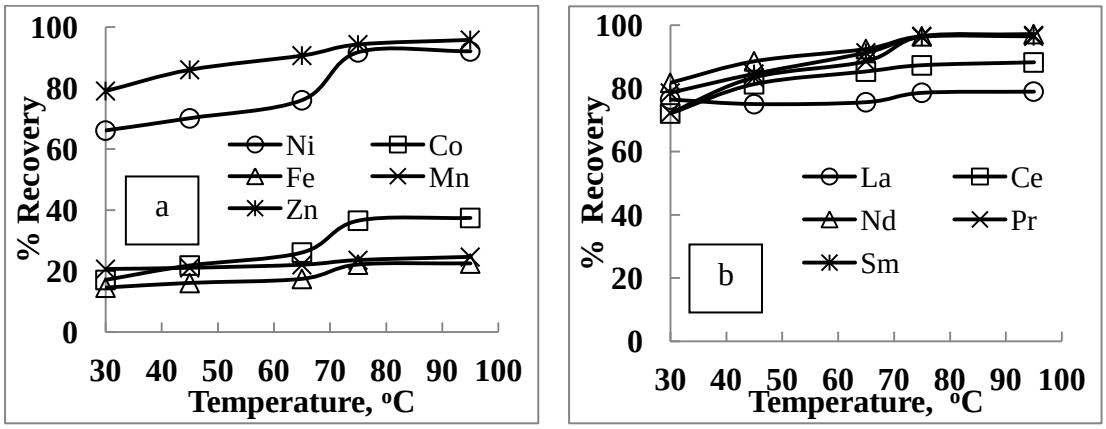

Fig. 4.26: Effect of temperature on leaching of (a) base metals, (b) rare earth metals from baked electrode material with 20 g/L PD in 60 min

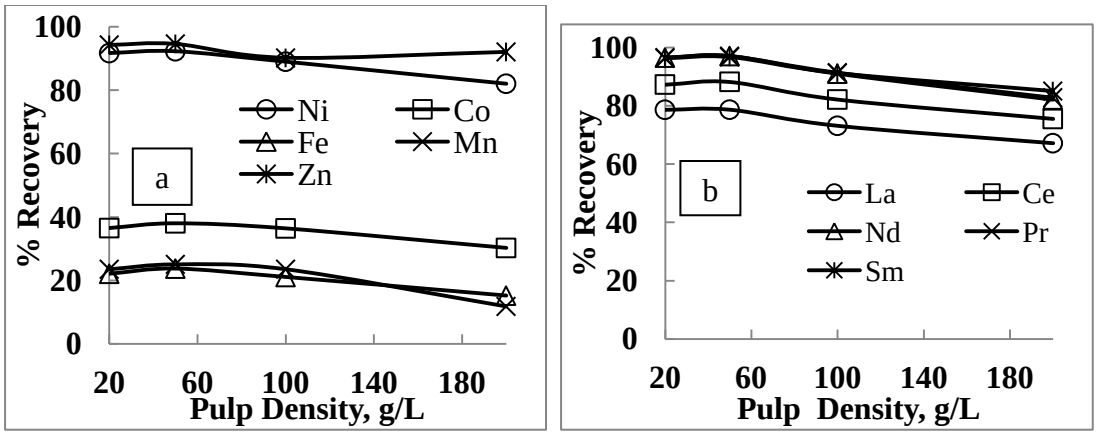

Fig. 4.27: Effect of pulp density on leaching of (a) base metals, (b) rare earth metals from baked electrode material at 75^{o}C in 60 min

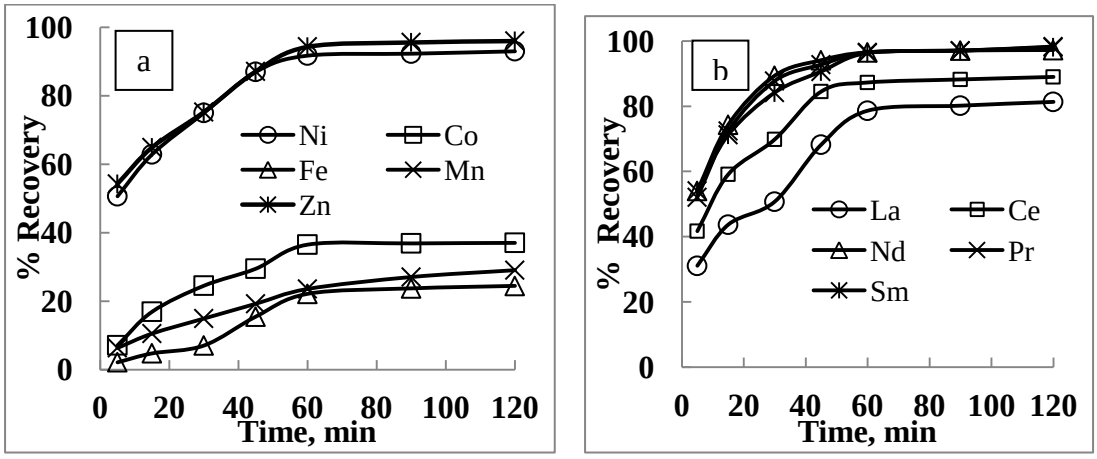

Fig. 4.28: Effect of time on leaching of (a) base metals, (b) rare earth metals from baked electrode material at 75^{o}C, 100 g/L PD in 60 min

It is necessary to understand the thermodynamics of reaction during the water leaching of the acid baked phases. After water leaching, the formation of dominant phases of Nd, Mn, Co makes these metals prevalent in the residue which can be identified by calculating the standard free energy change for the water leach reactions of baked material. Equations 4.11-4.17 describe the most likely reactions of Ni, Zn, Nd, La with water (leach-I) along with the ΔG^{o} at 348 K (HSC Chemistry 7.14). As can be seen, the major transformed phases ($NiSO_4$, $(NiFe)SO_4$, Nd_2S_3, $La_{2.607}S_4$, Nd_2Ni_7, $ZnSO_4$) present in the baked powder react with water improving the leaching of Ni, Zn, REs while converting Co, Mn to relatively less soluble or insoluble compounds (Eq. 4.16) at 348 K (75 ^{o}C). The ΔG^{o} values for Eqs. 4.13-4.17 clearly

demonstrate the thermodynamic feasibility of the water leach reactions (Table 4.8). The formation of Mn_2O_3 as per Eqn. 4.16 indicates the presence of manganese unleached after stage-1 which was analyzed to be the major phase (Table 4.5). The water leached residue rich in Co and Mn, was further subjected to leach-2 stage to recover the remaining metals.

$NiSO_4 = Ni^{2+}_{(a)} + SO_4^{2-}{}_{(a)}$ $\Delta G^o_{347K} = -18.3$ kJ (4.11)

$(NiFe)SO_4 + 2H^+_{(a)} = Ni^{2+}_{(a)} + Fe^{2+}_{(a)} + SO_4^{2-}{}_{(a)} + H_{2(g)},$ $\Delta G^o_{347K} = -80.152$ kJ (4.12)

$Nd_2S_3 + H_2O + 5.5O_{2(g)} = 2Nd^{2+}_{(a)} + 2H^+_{(a)} + 3\ SO_4^{2-}{}_{(a)},$ $\Delta G^o_{347K} = -1624.3$ kJ (4.13)

$La_{2.607}S_4 + 4\ H^+ = 2.607\ La + 4\ HS^+$ $\Delta G^o_{347K} = -2292.6$ kJ (4.14)

$Nd_2Ni_7 = 2Nd^{2+}_{(a)} + 7\ Ni^{2+}_{(a)} + 18e^-$ $\Delta G^o_{347K} = -20.3$ kJ (4.15)

$5MnS_{0.4}O_{2.6} + H_2O = 2Mn_2O_3 + 2H^+_{(a)} + 2SO_4^{-2}{}_{(a)} + Mn^{+2}_{(a)}$

$\Delta G^o_{348K} = -282.1$ kJ (4.16)

$ZnSO_4 + H_2O + O_2 = Zn^{2+} + 2H^+ + 3SO_{2(g)}$ $\Delta G^o_{347K} = -289$ kJ (4.17)

Table 4.8: ΔG^o for chemical reactions during baking of electrode material in temperature range 303-368 K

T (K)	ΔG^o values for the equations 4.11-4.17 (kJ)						
	Eqn 4.11	Eqn 4.12	Eqn 4.13	Eqn 4.14	Eqn 4.15	Eqn 4.16	Eqn 4.17
303	-29.4	-92.6	-1688.7	-2437.7	-23.1	-299.8	-266
318	-26.2	-88.7	-1668	-2392.6	-22.4	-294.4	-271
338	-21.4	-83.1	-1639.3	-2327.3	-21.1	-286.4	-280
348	-18.9	-80.2	-1624.4	-2292.5	-20.3	-282.1	-289
368	-13.5	-73.8	-1593.7	-2219.1	-18.5	-272.8	-291

4.3.3*. Second stage leaching (leach-II):* The results of the treatment of water leach residue (rich in cobalt and manganese) obtained above using different lixiviants are presented and discussed. The effect of acid concentrations on the leaching of Co and Mn from the leach-I residue generated at 75 ^oC, 50 g/L PD and 60 min, was tested. Initial experiments were carried out using the H_2SO_4 in the concentration range 0.5-2 M at 20 g/L pulp density and 95 ^oC. With 1 M H_2SO_4 the amounts of Co and Mn leached in the solution were <27-30 % (Table 4.9). Beyond 1 M sulfuric acid metal

recovery increased only marginally and therefore, this concentration was considered optimal. On adding a reducing agent viz., 0.1 M $NaHSO_3$ in 1 M H_2SO_4, leaching of cobalt and manganese improved to ~55% and 74% because of better solubility of their phases such as Mn_2O_3 and $CoS_{1.97}$ (Table 4.9). The increased recovery of cobalt is attributed to the fact that HSO_3^- ions can react with $CoOSO_4$ as shown in Eq. 4.18. The un-reacted Mn_2O_3 in leach-I residue also reacts with HSO_3^- ions in presence of H_2SO_4 as shown in Eqn. 4.19 dissolving manganese significantly.

$$CoOSO_4 + HSO_3^-{}_{(a)} = Co^{2+}{}_{(a)} + 2SO_4^{2-}{}_{(a)} + H^+{}_{(a)} \qquad \Delta G^o{}_{368K} = -183.75 \text{ kJ} \quad (4.18)$$

$$Mn_2O_3 + HSO_3^-{}_{(a)} + 3H^+{}_{(a)} = 2Mn^{2+}{}_{(a)} + SO_4^{2-}{}_{(a)} + 2H_2O, \ \Delta G^o{}_{368K} = -252.6 \text{ kJ} \quad (4.19)$$

$$Nd_2Ni_7 + 18HSO_3^-{}_{(a)} + 13.5O_{2(g)} = 2Nd^{2+}{}_{(a)} + 7Ni^+{}_{(a)} + 9H_2O + 18SO_4^{2-}{}_{(a)}$$

$$\Delta G^o{}_{368K} = -5638.8 \text{ kJ} \quad (4.20)$$

Eqs. 4.18-4.20 are quite feasible as the calculated values of Gibbs free energy change (HSC Chemistry 7.14) are highly negative at 368 K. The ΔG^o values reflect the prospects of leaching $CoOSO_4$, Mn_2O_3 and Nd_2Ni_7 by sulfuric acid in presence of sodium bisulphite. This explains for the high recovery of cobalt and manganese from the water leached residue in the stage-II (reductive acid leach). The remaining un-dissolved Nd (and possibly Sm also) of stage-1 are completely leached as per Eq. 4.20 adding to the recovery of the rare earth individually and collectively.

The two-stage leaching process, thus represents the leaching of the baked electrode material by water (leach-I) at 75 ^oC and 50 g/L PD for 60 min, followed by leaching with the $NaHSO_3$ in H_2SO_4 in leach-II at 95 ^oC and 20 g/L PD for the same duration. The baking-leaching process seems to be an alternate approach depending on the composition of electrode material which can ensure the selective dissolution of Ni, Zn and REs over other metals (Co and Mn) and the lower acid consumption compared to the direct sulfuric acid leaching. Increasing the acid concentration and lowering the

Table 4.9: Effect of acid, and reductant concentration on leaching of metals from residue of Leach-I at 20 g/L and 95 ^{o}C

Metals		% Recovery					
		0.5 M H_2SO_4		1 M H_2SO_4		2 M H_2SO_4	
		No reductant	0.1 M $NaHSO_3$	No reductant	0.1 M $NaHSO_3$	No reductant	0.1 M $NaHSO_3$
Ni		3.11	5.21	4.32	6.47	4.41	6.51
Co		26.2	39.4	38.88	54.89	39.76	55.12
Zn		2.1	3.2	2.7	3.7	2.8	3.9
Mn		29.67	66.2	40.22	74.27	41.09	75.33
Constituent REs	La	0.8	0.5	1.7	0.98	2.4	1.2
	Ce	8.22	5.66	11.49	6.43	12.11	7.15
	Nd	0.9	0.8	1.68	1.3	1.91	1.5
	Pr	0.9	0.72	1.96	1.28	2.13	1.35
	Sm	1.09	0.92	2.86	1.36	3.1	1.55

reaction temperature below 50 ^{o}C could result in high La dissolution (Sinha et al. 2016). The overall recovery in the two-stage leaching of the baked material could be worked out as Ni (98.2%), Co (91.39%), Zn (98%), Mn (97.77%) and REs (96%). The recovery of constituent REs was observed to be 80.35% La, 98.8% Ce, 98.2% Nd, 98.5% Pr and 99.2% Sm in 60 min.

4.3.4. *Material characterization*: The leach residues obtained from the treatment of the electrode material were characterized using XRD analysis (Fig. 4.29). In the untreated sample, the major [$Ni(OH)_2$, $LaNi_5$, Nd_2Ni_7, Ni, Co_2NiO_4] and minor phases [$CeCO_3$, Sm_2Fe_{17}, Ce_2Ni_7, $NiMn_2O_4$ and (Ni, Zn) Fe_2O_4] identified (Fig. 2.6; Table 2.4) can change as a result of processing. Baking of the material in 90 min produced relatively friable powder, in which the reaction with sulfuric acid led to the conversion of metals to respective sulfates /sulfites like $NiSO_4$, $(Ni,Fe)SO_4$, Nd_2S_3, Nd_2Ni_7, $La_{2.607}S_4$, and $ZnSO_4$ as the major phases while CeS, NiSm, Fe_5Sm, Sm_2O_2S, $Nd_2(SO_4)_3$, $CoS_{1.97}$ and $MnS_{0.4}O_{2.6}$ being the minor phases as established by the XRD analysis (Fig. 4.29a). The phases transformed during the acid baking account for the selective leaching of Ni, Zn and REs over Co and Mn in water leaching (leach-I). The XRD patterns (Fig. 4.29) and the phases identified (Table 4.5) show the progressive decrease in intensities of the major peaks for the residues collected as the time

elapsed. The Ni-Zn-REs depleted leach-I residue after water leaching at 75 ^{o}C for 120 min shows the presence of Nd_2Ni_7 and Mn_2O_3 as the major phases along with Co rich phases such as Sm_2Co_7, $CoS_{1.97}$ and $CoO.SO_4$. The selective dissolution of Ni, Zn and REs is illustrated by the decreased ratio (minor phase) of these metals with a lower stoichiometric phase viz., NiO (Fig. 4.29b).The leach-II residue after reductive leaching with $NaHSO_3$-H_2SO_4 at 95 ^{o}C exhibits nearly complete dissolution of Co and Mn in 60 min (Table 4.7).

The leaching of metals with time was further examined by comparing the morphological changes through the FESEM studies and also the elemental distribution in the leach residues with that of the untreated sample (Figs. 4.30-4.33). EDAX data clearly show a progressive decrease in the average content of most metals (Ni, Co, Zn, Mn, REs) in the residues as the leaching proceeded in 2-stages. Fig. 4.30 (SEM) reflects the image of the untreated sample with larger particles present in irregular morphologies. The baked powder at the 300 ^{o}C depicts a porous rod like structure with the formation of new phases (Fig. 4.31). The leach-I residue after water leach (performed at 75 ^{o}C for 120 min) shows the lower concentration of Ni, Zn in EDAX, which further indicates the selective dissolution with corroded surface of the porous residue rich in Co and Mn (Fig. 4.32). High recovery of Co and Mn, besides the leaching of remaining Ni, Zn and REs, is corroborated by the decreased particle size (SEM, Fig. 4.33), and low elemental distribution (EDAX) in the leach-II residue. The characterization by XRD and SEM-EDAX studies thus provides evidence for the selective leaching of the metals in a two-step process.

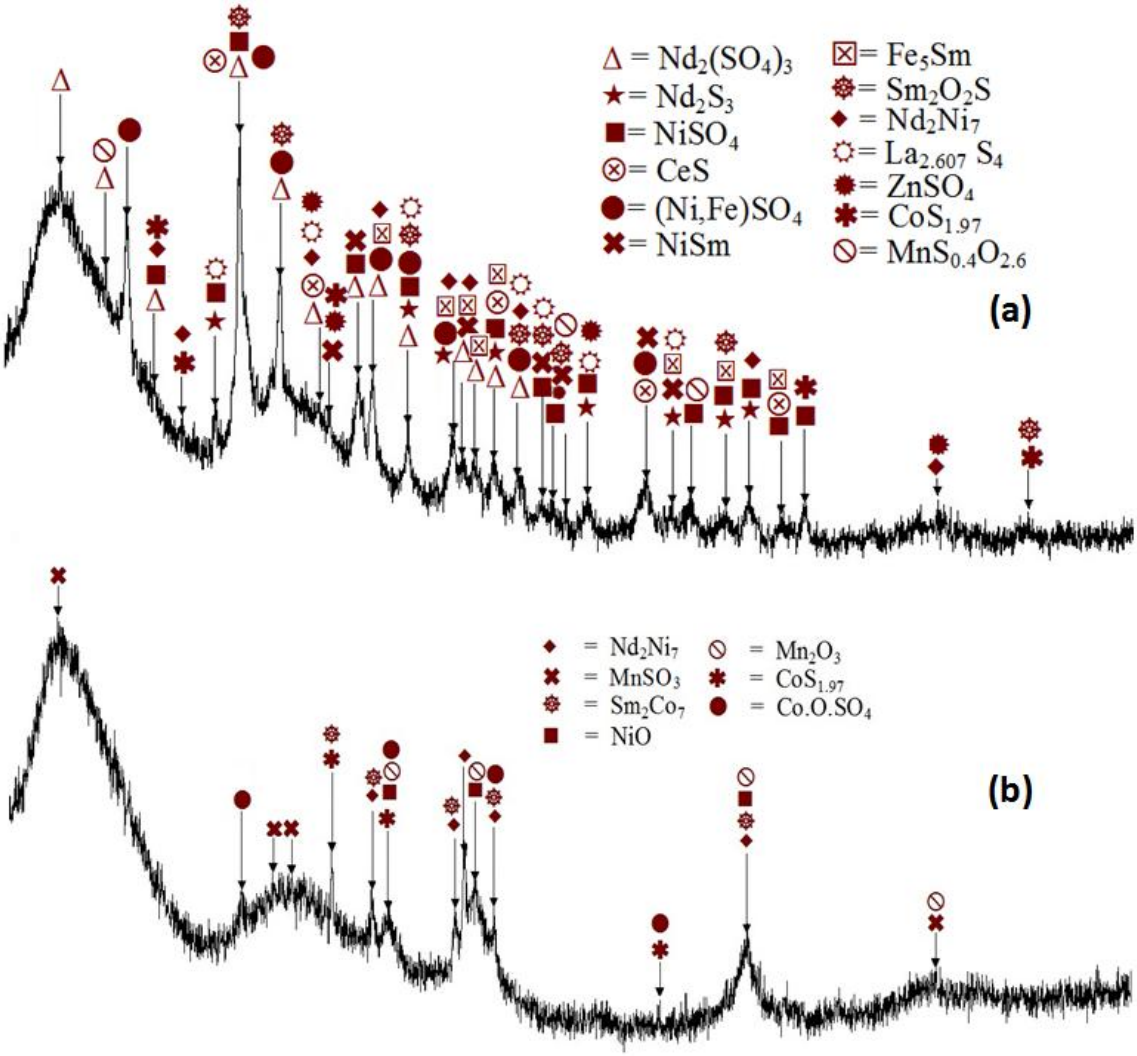

Fig. 4.29: XRD phase analysis of (a) baked electrode material; (b) 1st stage water leached residue

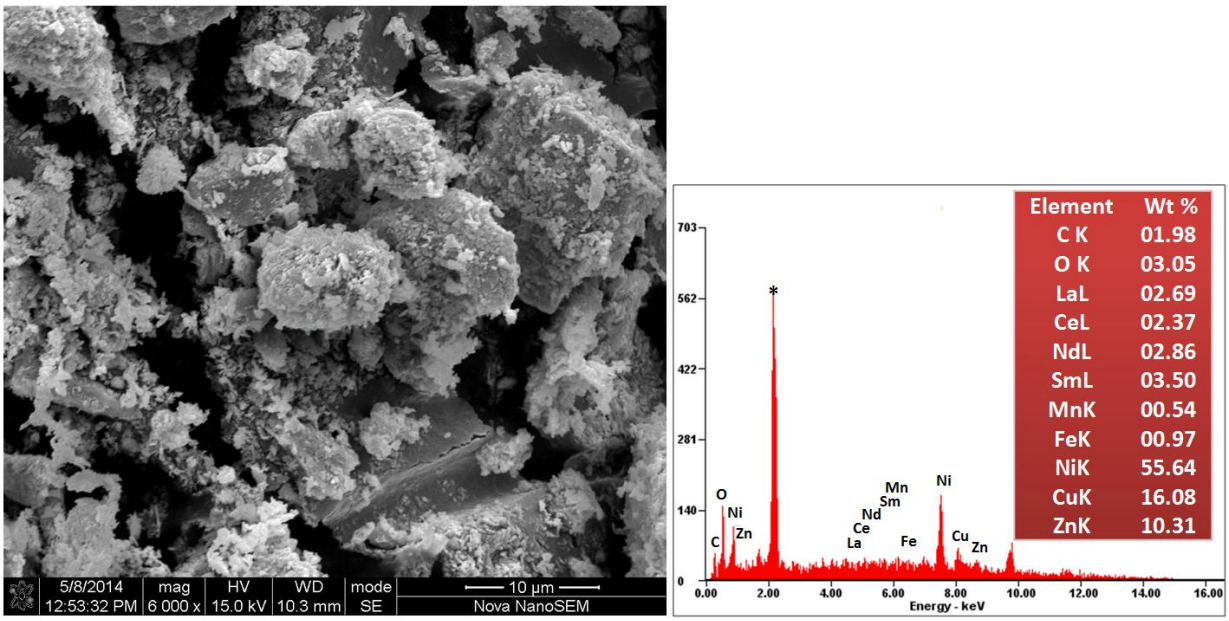

Fig. 4.30: SEM-EDAX analysis of untreated electrode material (* - Ag coating)

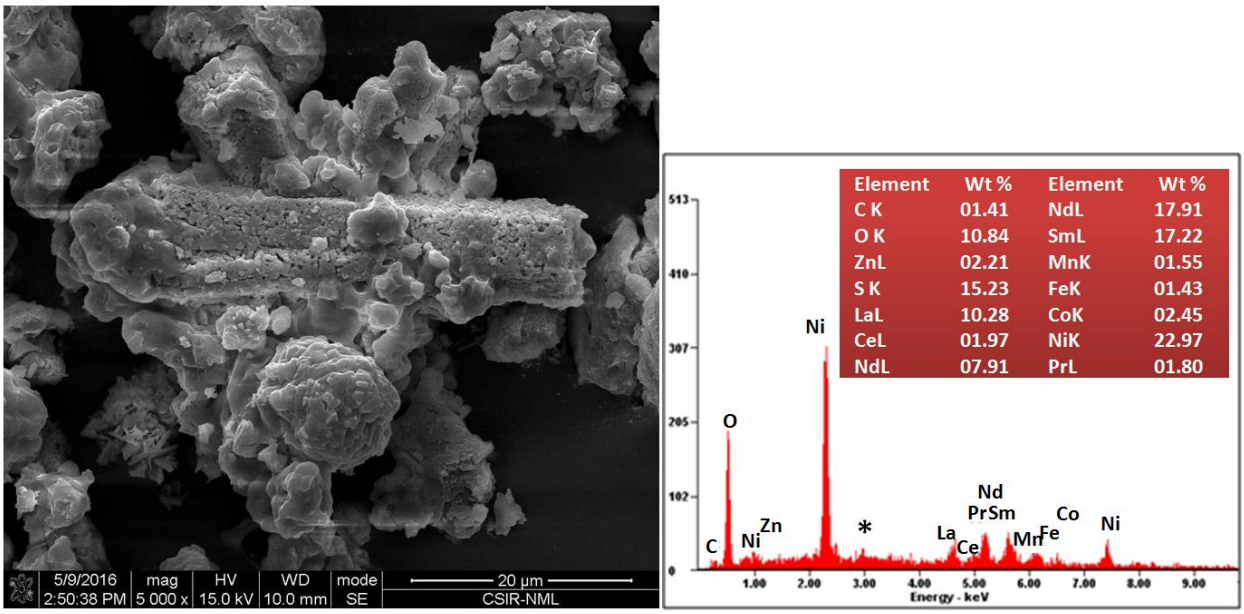

Fig. 4.31: SEM-EDAX analysis of baked electrode material (baking temperature: 300 ^{o}C, time: 90 min, acid: 1.5 mL H_2SO_4/2 g material; * - Ag coating)

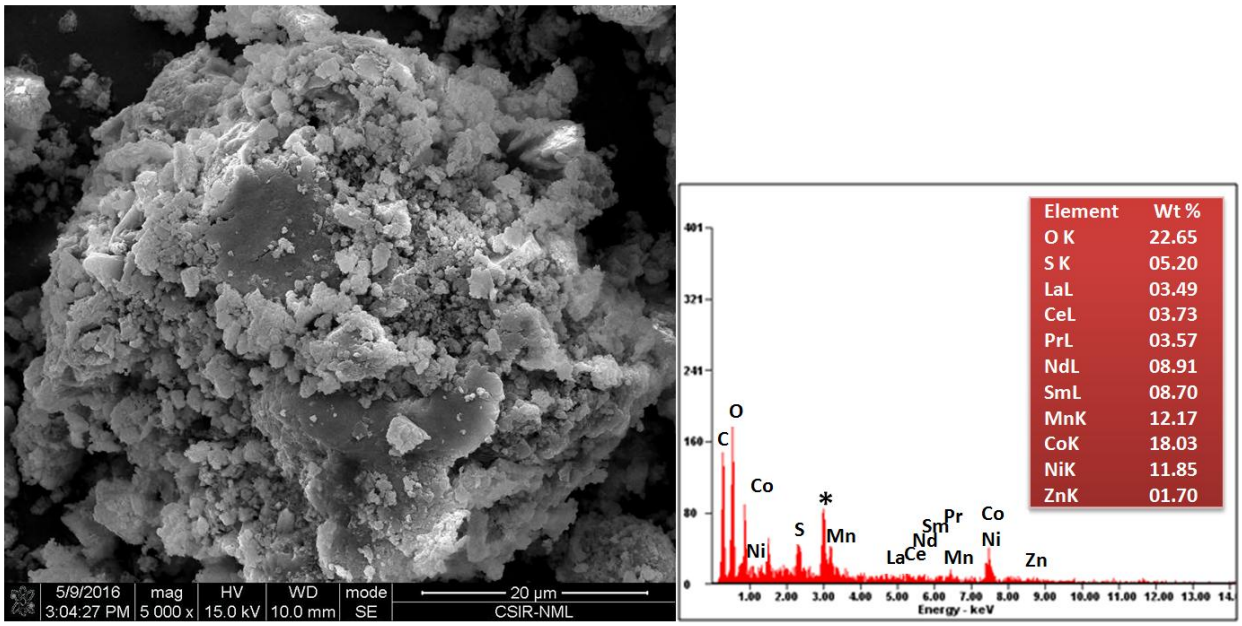

Fig. 4.32: SEM-EDAX analysis of leach-I residue after water leaching of baked material (75 ^{o}C and 100 g/L PD for 120 min; * - Ag coating)

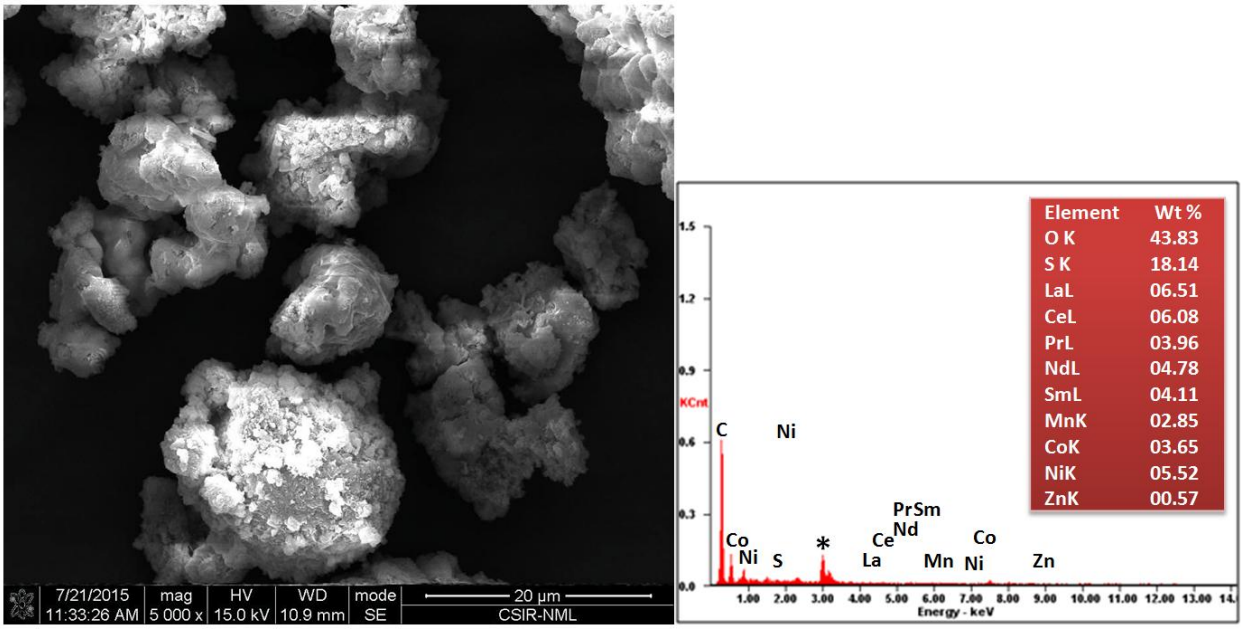

Fig. 4.33: SEM-EDAX analysis of residue obtained after leach-II (2nd stage leaching) in 60 min (1 M H_2SO_4 + 0.1 M $NaHSO_3$, 95^{o}C, 50 g/L PD; * - Ag coating)

Highlights

- Both the base metals (Ni, Co, Zn and Mn) as well as rare earth metals (La, Ce, Pr, Nd and Sm) can be effectively recovered from the spent NiMH batteries by leaching in sulfuric acid.
- Leaching efficiency of base metals to the tune of 91.6% Ni, 97.8% Co, 93.5% Mn, 99.2% Zn and 65.5% Fe is attained with 2 M H_2SO_4 at 348 K, 100 g/L pulp density in 120 min.
- Leaching of rare earth metals can also be achieved simultaneously with the base metals under the similar conditions mentioned above with the recovery of 69.5% La, 98.1% Nd, 98.4% Sm, 95.5% Pr and 89.4% Ce.
- Leaching kinetics followed the chemical control shrinking core model for all the individual base and REs together, besides the individual rare earth metals. The kinetics of the metal dissolution have been supported by establishing the feasibility of reactions through the thermodynamics by calculating the change in the standard free energy (ΔG^o) and confirmed by the XRD phase identification and morphological changes (SEM-EDAX studies).
- The leaching of Ni, Co, Fe, Mn and Zn acquired the activation energy of 8.7, 6.8, 7.12, 6.7 and 7.9 kJ /mol, respectively in the temperature range 305-348 K. Similarly the leaching of rare earth metals viz. Nd, Sm, Pr and Ce acquired the activation energy of 7.6, 6.3, 11.3 and 13.5 kJ /mol, respectively.
- Process intensification by baking of NiMH battery powder at 300 °C, 1.5 mL H_2SO_4 /2 g powder and 90 min, followed by the water leaching (leach-I) selectively recovers Ni (91.7%), Zn (94.3%) and REs (93%) over metals such as Co (36.5%) and Mn (23.5%) while showing the low acid consumption as compared to direct sulphuric acid leaching. Leach-II using sodium bisulfite in sulfuric acid could recover Co and Mn and the residual Ni and Zn under the mild leaching conditions.
- The overall recovery in the two-stage leaching of the baked electrode powder is worked out as: 98.2% Ni, 91.39% Co, 98% Zn, 97.8% Mn and 96% REs. The leaching efficiency of the constituent REs is found to be 80.35% La, 98.8% Ce, 98.2% Nd, 98.5% Pr and 99.2% Sm.